1-1-2011

Measurement and Characterization of Terahertz Radiation Propagating Through a Parallel Plate Waveguide

Matthew George Wachsmuth
Portland State University

Let us know how access to this document benefits you.

Follow this and additional works at: http://pdxscholar.library.pdx.edu/open_access_etds

Part of the Electrical and Computer Engineering Commons

Measurement and Characterization of Terahertz Radiation Propagating Through a

Parallel Plate Waveguide

by

Matthew George Wachsmuth

A thesis submitted in partial fulfillment of the
requirements for the degree of

Master of Science
in
Electrical and Computer Engineering

Thesis Committee:
Branimir Pejcinovic
Robert Daasch
Martin Siderius

Portland State University
©2011

Abstract

As the amount of study into the terahertz (THz) region of the electromagnetic spectrum steadily increases, the parallel plate waveguide has emerged as a simple and effective fixture to perform many experiments. The ability to concentrate THz radiation into a small area or volume enables us to analyze smaller samples and perform more repeatable measurements, which is essential for future research. While the fundamental physics of PPW transmission are understood mathematically, the practical knowledge of building such a fixture for the THz domain and taking measurements on it with a real system needs to be built up through experience.

In this thesis, multiple PPW configurations are built and tested. These include waveguides of different lengths and opening heights, using lenses and antennas to focus and collect radiation from the input and output, and different amounts of polish on the waveguide surface. A basic resonator structure is also built and measured as a proof of concept for future research. The two most useful propagation modes through the waveguide, the lowest order transverse magnetic (TEM) and transverse electric (TE) modes, were characterized on all of the setups. Additionally, a flexible fixture was designed and measured which will allow future work in the THz field to be much more reliable and repeatable.

Table of Contents

List of Tables

List of Figures

I.   Introduction

Before the experiments detailed in this thesis can be explained, a basic introduction to the

terahertz spectrum and the fundamentals of electromagnetic propagation will be

discussed. This will be followed by a list of experiments performed during the course of

the research, their results, and conclusions from the results. Finally, future work to be

done based on the results and conclusions will be detailed.

A.   Introduction to Terahertz Research

The field of terahertz (THz) research is a new area of study and thus creates a challenging

arena in which to work. The THz band, usually defined as the frequency space between

0.3THz to 3THz, has many potential applications. These include medicine, biology,

security, material sciences, chemical engineering, with more uses being found all the

time. Only in the past 10 years has the THz spectrum begun to be closely studied due to

recent advances in radiation generation and measurement capabilities. The research done

in this thesis and in other recent papers represents the foundation for which further

important research will be conducted on.

Figure I.1 shows the area of interest in the electromagnetic spectrum, between

microwaves and infrared light.
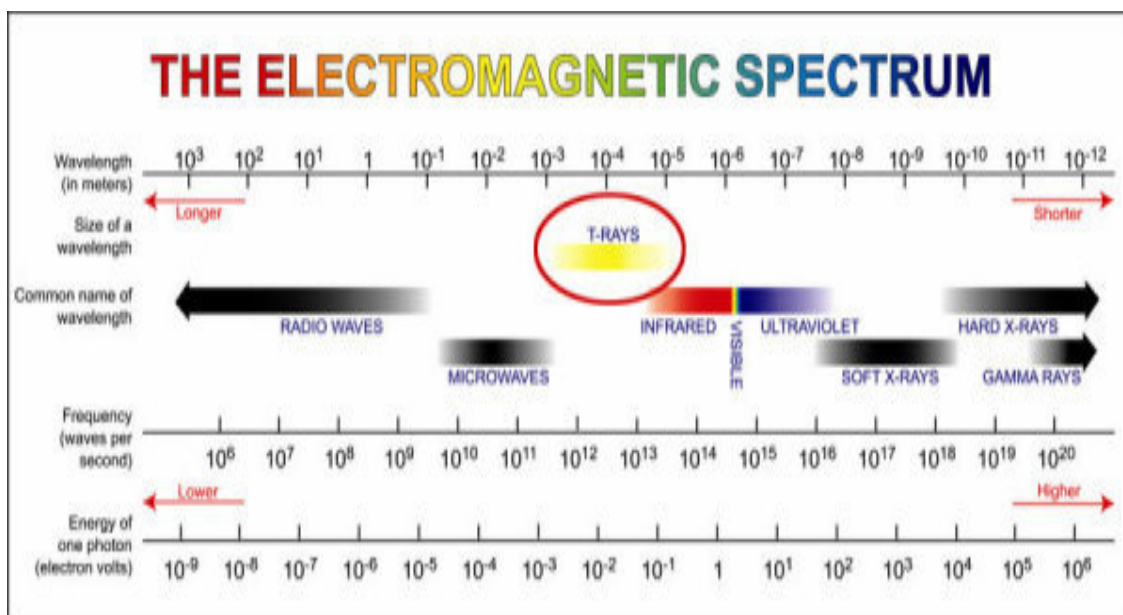
Figure I.1: The EM spectrum with the THz domain circle[1]

It is important to note that because THz radiation lies between the electronic and optical domains, the simple assumptions used in either domain (such as ignoring scattering times and atmospheric losses, the skin effect, etc) no longer hold true. This is part of the challenge of working in the THz part of the spectrum, and why it is necessary to perform a large amount of experimentation.

B.   Generating Terahertz Radiation

One of the problems with THz research is generating reliable, powerful, and accurate sources. Creating radiation in the THz range by electronic means is hampered due to the

---

[1] Image taken from www.socialtext.net/ism4300/index.cgi?thruvision_s_t5000_camera

$1/f^2$ falloff shown in figure I.2. Additionally, optical sources also drop off in power and ability in the THz range as shown in the figure. Only recently have sources become available that are flexible and fast enough to use for THz research.
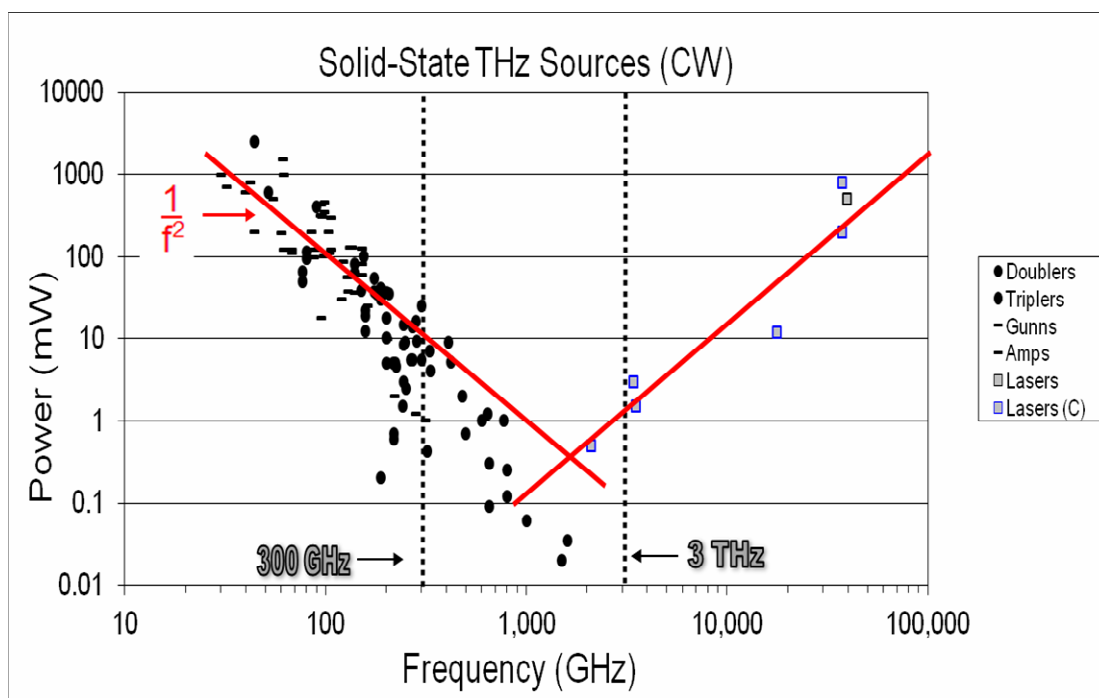
Figure I.2: Frequency vs. power for continuous-wave THz sources[2]

Both optical and electronic means can be used to generate THz radiation, but each method uses different approaches to either down convert from the optical range or up convert from the microwave spectrum. Also, the method is different depending on if continuous wave (CW) radiation is being produced or a broadband pulse in the THz spectrum is being generated. Figure I.3 is a schematic representation of how these signals can be generated using crystals and diodes [16].

[2] Data courtesy of Virginia Diodes, Inc.
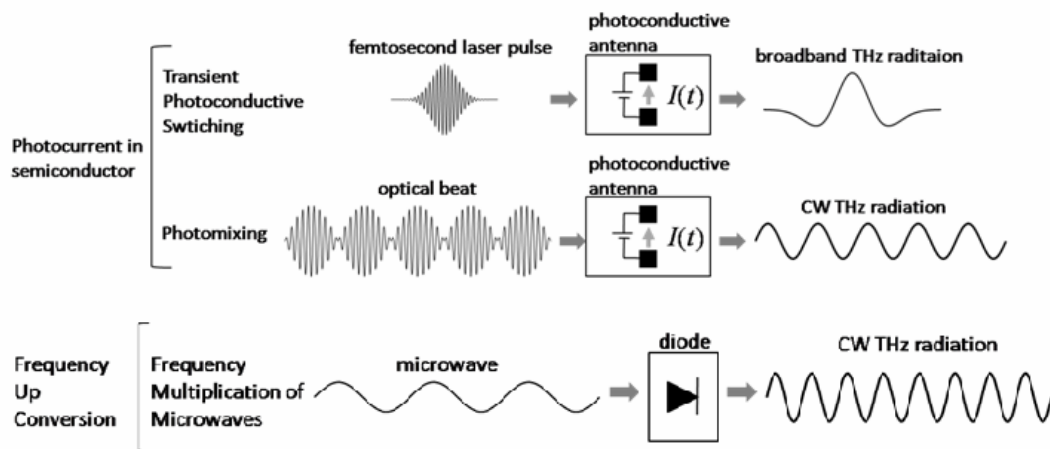
Figure I.3: Block diagram of THz radiation generation [16]

C.   THz Measurement Systems at Portland State University

The Portland State University Northwest Electromagnetics and Acoustic Research (NEAR) Lab has the capability to perform time-domain spectroscopy (TDS) as well as continuous wave (CW) measurements in the THz range. While all of the measurements in this thesis were taken with the TDS system, the fundamentals learned on parallel plate transmission will apply to the CW system as well.

i.   Time-Domain System

The T-Ray 4000 manufactured by Picometrix was used to perform all measurements in
this thesis. Figure I.4 shows a picture of the measurement equipment along with the
transmit and receive heads.

Figure I.4: Picometrix T-Ray 4000 System (picometrix.com)

This system is a complete self-contained generation and measurement tool that makes all
THz-related measurements very simple. The software performs real-time FFT of the
received THz pulse, and also allows for averaging. The bandwidth specified on the
Picometrix website is from 0.02 to 2THz (with an option for up to 3THz) with a peak

SNR of 70dB. The heads allow for focusing lenses to be used as well, for higher-precision tasks where precise placement of THz radiation (like at the input of a waveguide) is necessary. The THz signal produced by this instrument is of the pulsed variety described at the top of Figure I.3, with a pulse duration of around 5ps. This type of system is often described as a THz time-domain spectrometer (TDS) but it is important to realize that it measures not only amplitude of the signal but also its phase.

ii.   Frequency Domain System

An example of a setup employing CW THz radiation (as opposed to the Picometrix which uses a broadband pulse and THz-time domain spectroscopy) would be the other system in the NEAR lab, produced by Virginia Diodes Incorporated (VDI). The system uses a 40GHz VNA with extenders (through the use of doublers and triplers) to provide a frequency range of 0.07THz up to 0.7THz. The advantages of this setup is the ability to measure S parameters (including reflection), and thus to better characterize devices (active devices in particular) and materials. Figure I.5 shows an example schematic for a specific band.
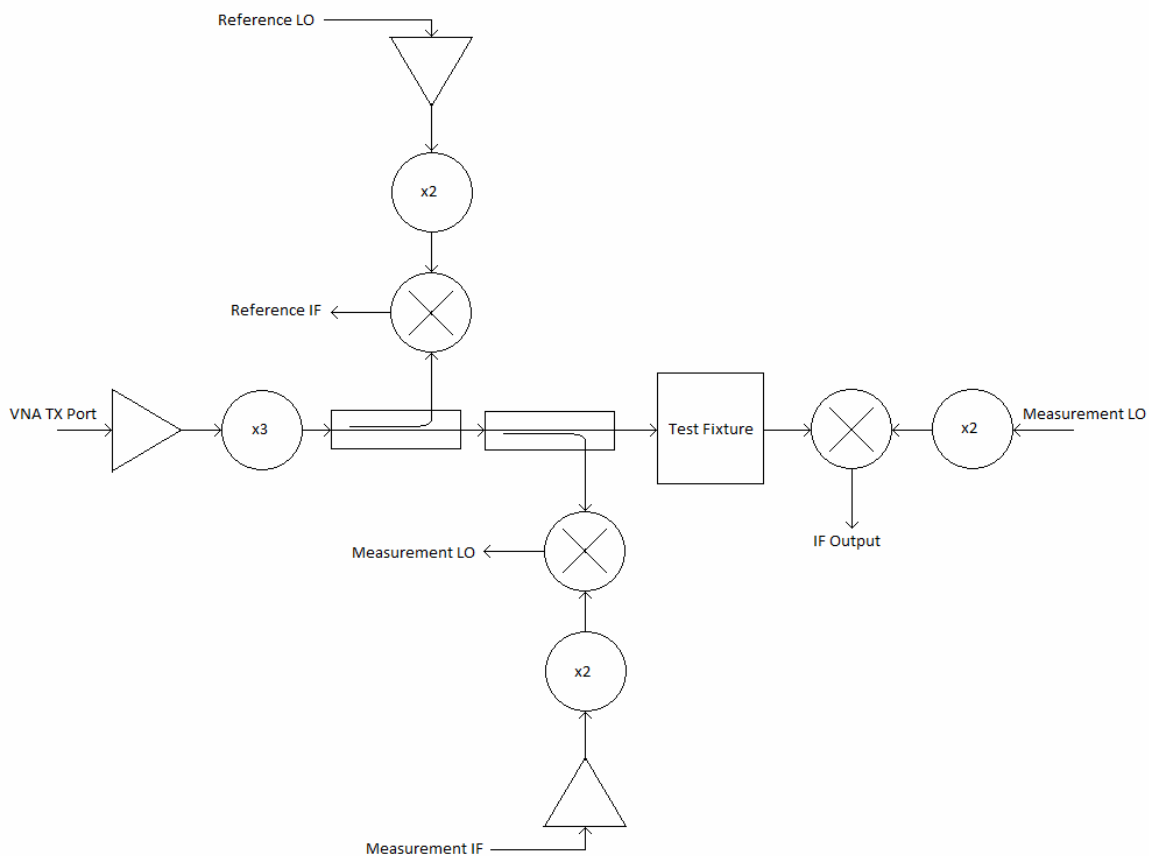
Figure I.5: Diagram for VDI system to measure in frequency range of 110-170GHz[3]

Figure I.6 is a picture of the VDI setup in the Portland State University NEAR lab. The two orange objects in the foreground are the transmit/receive antennas, and the items behind them are the doublers/triplers which up convert the microwave radiation into the appropriate range, and down convert the THz radiation back down.

---

[3] Data courtesy of Virginia Diodes, Inc.
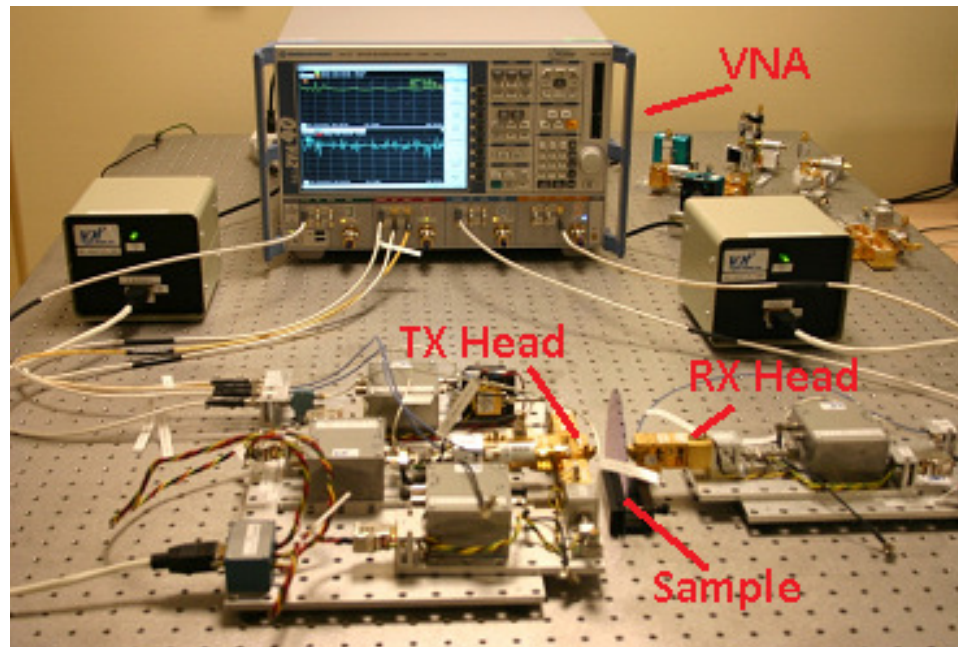
Figure I.6: Picture of VDI THz CW system

D.   Applications of Terahertz

There are many different applications that involve THz radiation, and below are a few examples. One reason why THz radiation is so useful is because it is non-ionizing, so items can be analyzed without damaging them (as opposed to x-rays). Also, many molecules have vibrational and/or rotational modes in the THz region, and thus differences between molecules can be determined when excited with radiation in the THz spectrum.

i.   Imaging

Probably the most mainstream application of this technology is that of imaging. Because

of the small wavelength, fine details can be observed. Besides using imaging for security

purposes, it can also be used for things like quality control on an assembly line to make

sure an item is being produced properly. Figure I.7 is an image of a chocolate bar imaged

with THz, along with a man imaged with a THz security system in figure I.8. One

interesting thing to note in figure I.8 is that different materials react with the radiation

differently. Hair and clothing are nearly transparent, while metal shows up as black, and

plastic (the frame of the handgun on his back) shows up as almost the same color as his

skin.
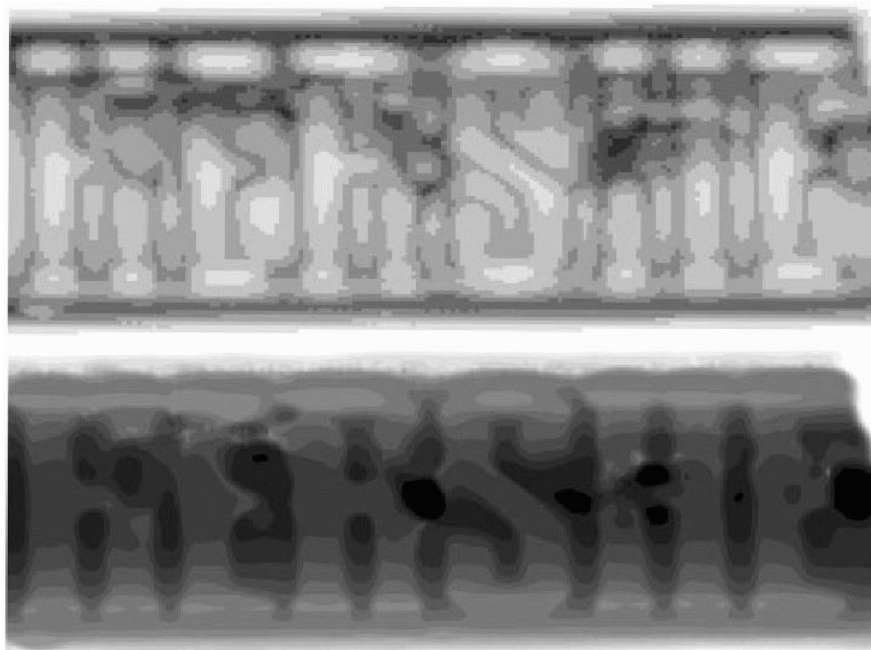
Figure I.7: Chocolate bar imaged with THz[4]

_____

[4] Image from www.thznetwork.net
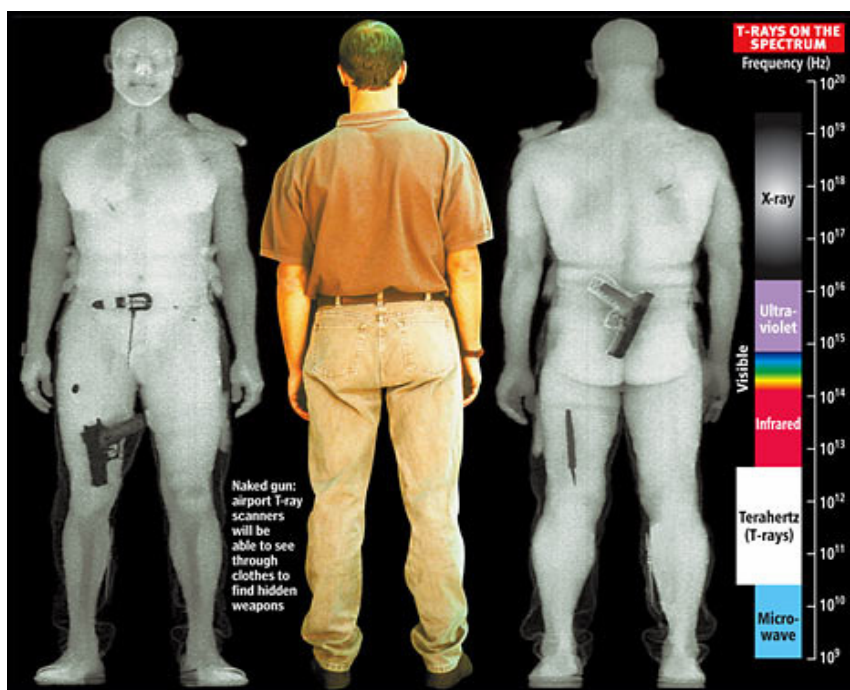
Figure I.8: Man imaged with THz[5]

ii.   Materials Detection

As mentioned previously, many molecules react to THz radiation, and these reactions can show up in the frequency domain as absorption of a specific frequency or set of frequencies. This means that there is a lot of potential to non-destructively analyze a sample and know what the molecular structure is. An example of this is detailed in [10]. In this paper, they cut a small groove into a waveguide and measured the resonant frequency created by the groove (the blue plot in the figure I.9). Fluids were then run through the groove and measured the change in the resonant frequency (labeled as ΔRF in the figure).

---

[5] Image from http://www.socialtext.net/ism4300/index.cgi?thruvision_s_t5000_camera
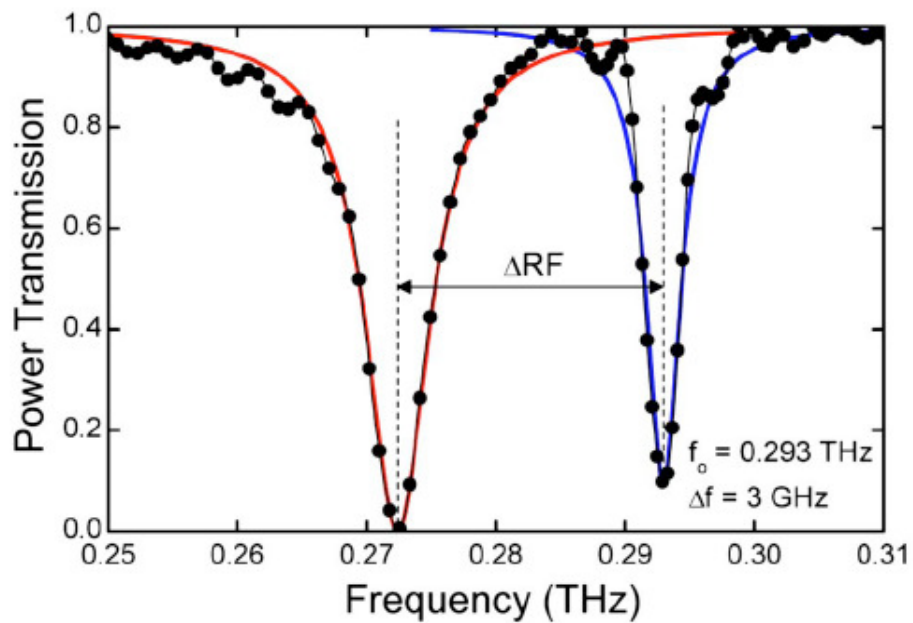
Figure I.9: Transmission through a waveguide notch [10]

Several similar fluids starting with C_8H_{18} (octane) up to $C_{16}H_{34}$ (hexadecane) were used, and the slight variation in resonance was plotted as shown in the figure I.10. As can be seen, there is a very noticeable difference between each fluid used.
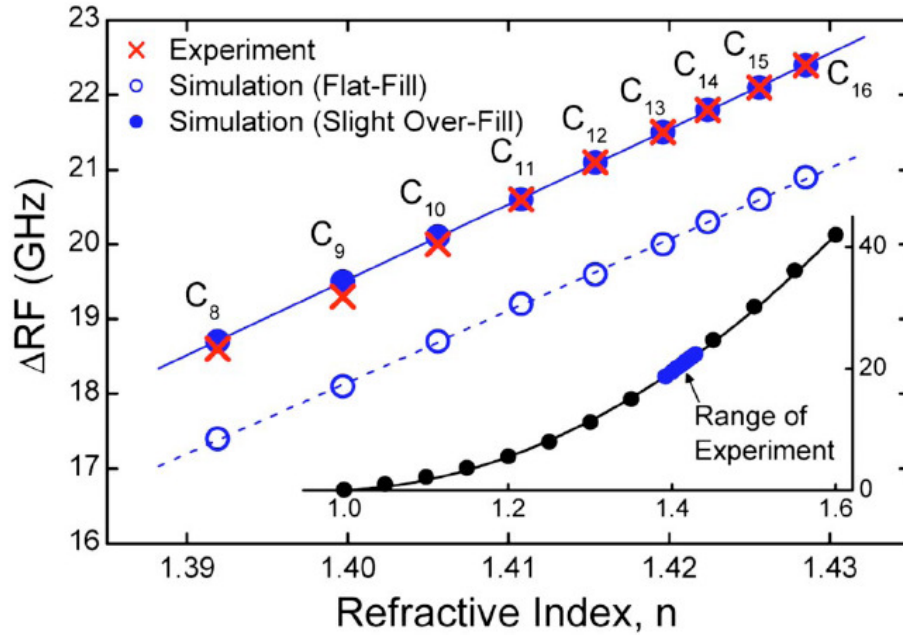
Figure I.10: Change in resonant frequency vs. refractive index for different liquids [10]

The applications for such a process are numerous, as it could be used to monitor liquids in real time as they flow by a THz transmitter/receiver. Many other materials have their own resonant shape, lactose powder being one that the Portland State NEAR lab studies quite often.   Figure I.11 is a plot of lactose in a waveguide versus air. As can be observed, there is a very large dip at around 0.5THz, followed by a steep high-frequency fall-off at around 1.1THz. There are also several dips across the frequency band that are caused by water vapor absorption. These water vapor peaks, some of which are listed in table I.1, will be present for all measurements described in this thesis.

Table I.1: Water vapor peaks from 0.2-1.5THz [17]

Water vapor absorption frequencies (THz)								
0.557	0.752	0.988	1.097	1.113	1.163	1.208	1.229	1.41
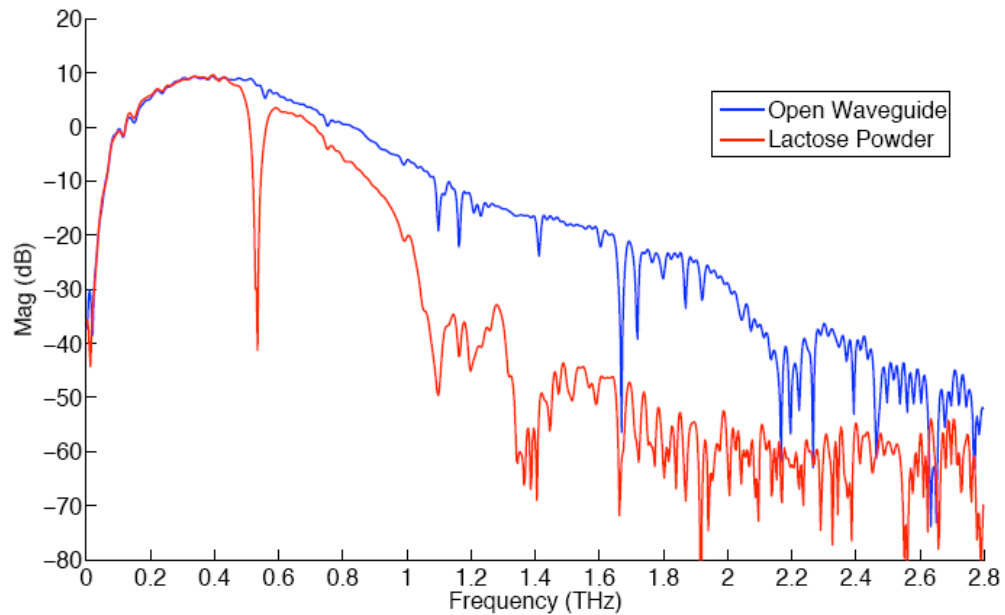
Figure I.11: Measured signal through a PPW filled with air and lactose

iii.   Medicine

A combination of imaging and materials detection can be used in the medical field to

perform a variety of tasks. An example of this is figure I.12, where a tooth scanned with

THz radiation can be analyzed to check for cavities. The technology currently used to do

this (X-Rays) is hazardous to people because it uses ionizing radiation, so terahertz could

be used as a much safer way to perform the same task. A company which sells

equipment to perform this, TeraView, claims that the TeraView system "is able to

distinguish between the different types of tissue in a human tooth; detect caries at an

early stage in the enamel layers of human teeth and monitor early erosion of the enamel

at the surface of the tooth."
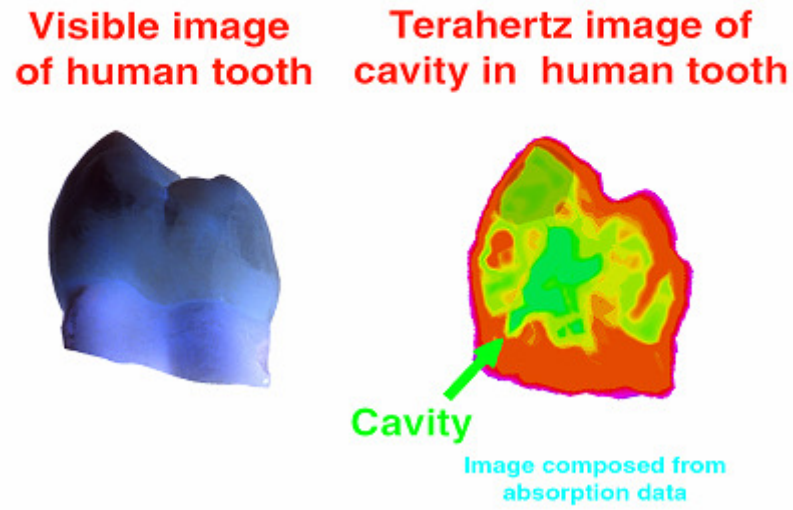
Figure I.12: Normal image vs. THz image of a tooth with cavity[6]

iv.   Integrated Circuit Analysis

A new application just put forth by Intel and TeraView is using THz waves to perform a failure analysis time-domain reflectometry (TDR) on integrated circuit packages. Because of the high frequencies used, faults can be found by using reflections to within a very small area. The press release from Teraview states "The technique, which utilises TeraView's proprietary Terahertz Pulse technology (TPI[TM]), isolates faults on interconnects to within 10 microns, enabling production and quality issues to be rapidly identified and addressed. The tool reduces failure analysis times from days to minutes and enables fault isolation in packages where conventional FA tools have failed."

---

[6] Image taken from www.teraview.com/terahertz/id/35

II.   Theory

A.   Terahertz Time-Domain Spectroscopy

The only measurement method used in this thesis was terahertz time-domain spectroscopy (THz-TDS). In THz-TDS, a single pulse (usually several picoseconds long) is outputted by the transmitter, and the receiver picks it up after a certain amount of transit time. Certain materials between the transmitter and receiver may increase the transmit time without significantly changing the signal amplitude or shape, while others may only attenuate it, or have some other effect such as scattering. A basic picture of a typical THz-TDS pulse is shown in figure II.1.
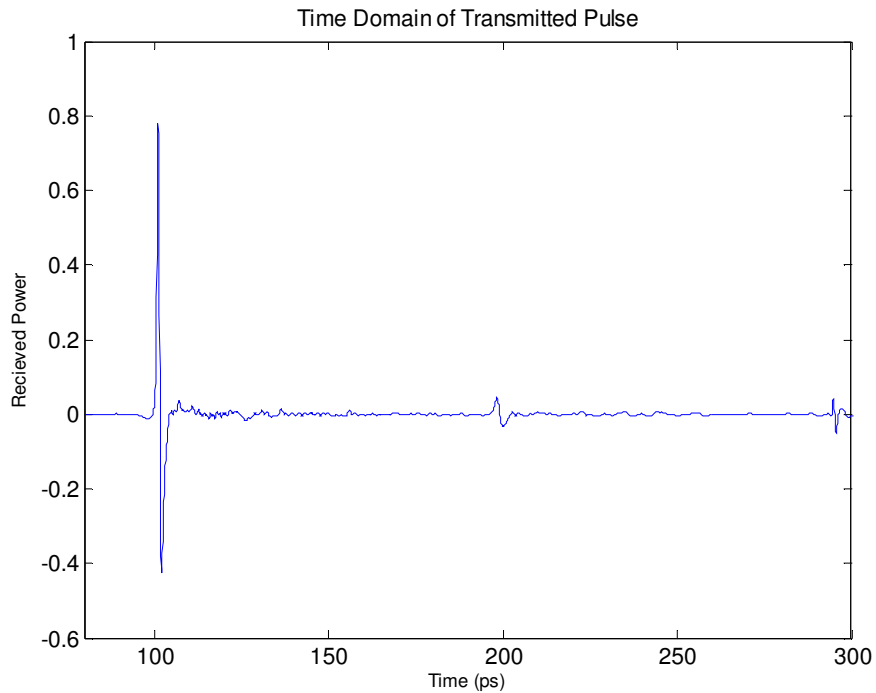
Figure II.1: THz time-domain pulse

Once this data is received in the time domain, an FFT can be performed on it to view it in the frequency domain. In most of the experiments detailed in this paper, the frequency domain was the more useful set of data to analyze. In reality, many pulses are transmitted and measured, and then averaged together. This has the effect of lowering the noise floor in the frequency domain. In figure II.1, 6000 samples were used. The fast Fourier transform (FFT) of figure II.1 is shown in figure II.2.
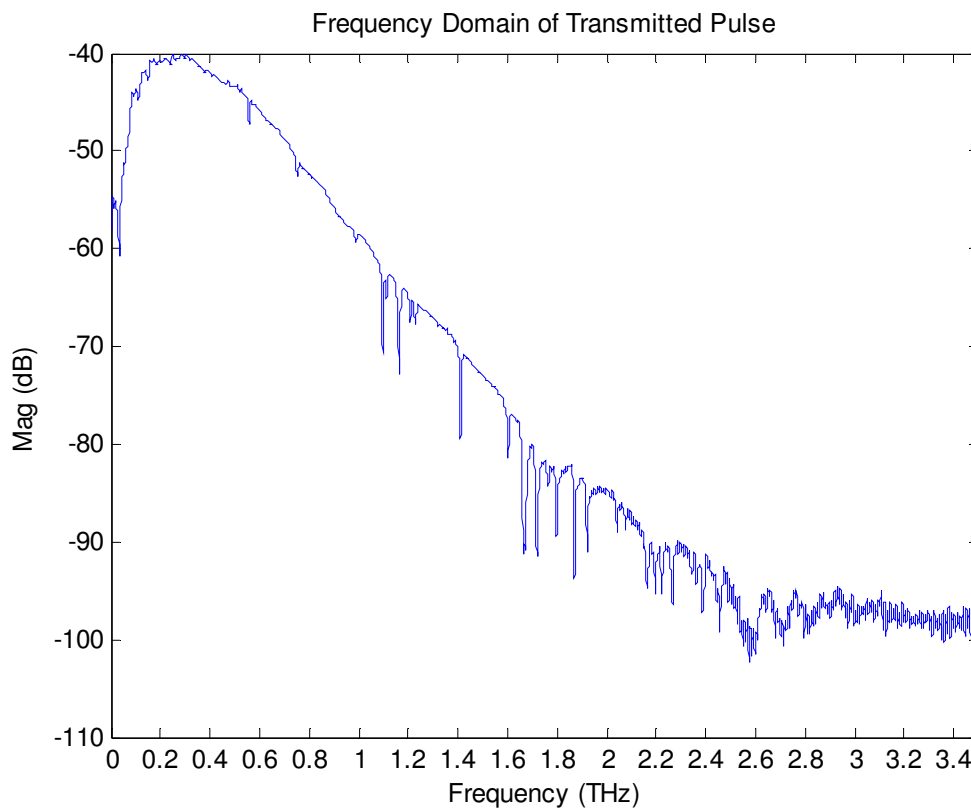
Figure II.2: Frequency spectrum of time-domain pulse of figure I.1

When working with a single pulse in THz-TDS, one important factor to consider is the window within which the data is analyzed. Many times there can be reflections along with the main received pulse that are delayed (observed in figure II.1 at 200 and 300ps),

and the maximum time that the instrument captures over is 320ps. As can be seen in

figure II.1, the third reflection is almost at 320ps, meaning any other received reflections

are getting cut out of the data, or even being received in the next time window.

Reflections can be caused by many factors, and in the case of figure II.1 they are caused

by radiation bouncing off of the metal casings on the outside of the transmit and receive

heads. In practice, reflections may contain useful information, so an appropriate window

of the data to be analyzed needs to be considered.

B.   Electromagnetic Wave Propagation

Even though this is a relatively new field of research, terahertz radiation still follows the

same laws of physics as any other electromagnetic wave. Maxwell's equations can be

used to fully comprehend the behavior of THz as it propagates through a medium. Figure

II.3 shows a transverse electromagnetic wave (TEM) propagating through free space over

two wavelengths.
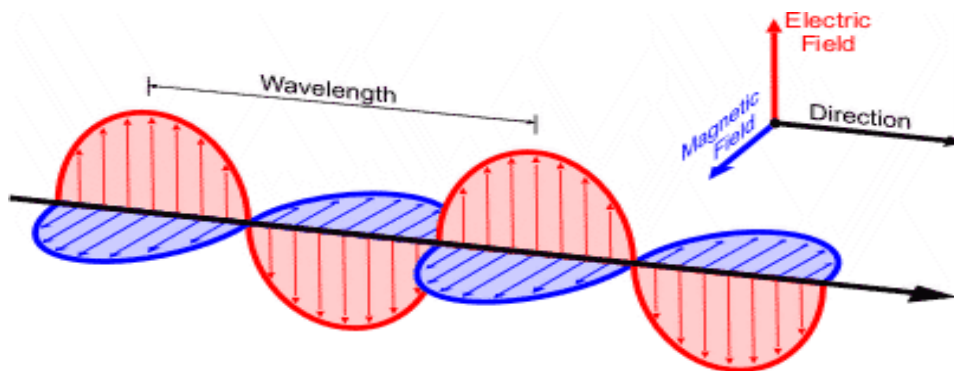
Figure II.3: TEM wave propagating through free space[7]

---

[7] Image taken from www.visionlearning.com

As one can see, the electric field is perpendicular to the direction of travel and the magnetic field. All of the THz radiation emitted by the Picometrix system used in the experiments is polarized in a similar fashion as in figure II.3. Depending on the orientation of the waveguide, the polarization will change so that either a TE wave or a TM wave propagates through the waveguide [6]. Schematically, the transmit head for the Picometrix would be on the origin of the axis, and the receive head would be at the other end of the direction of travel.

C.   Parallel Plate Waveguide Theory

Because parallel plate waveguides (PPW) are the main focus of study in this paper, a basic understanding of their use and reasons for use is necessary. A PPW represents the most basic and simple form of a guided electromagnetic wave interface. They can be very simple in design (and thus cheap to manufacture), but can be extremely useful in this field of study.

i.   Propagation Through a Parallel Plate Waveguide

The formulas that model how radiation propagates through a PPW can be greatly simplified with the approximation that the width is much larger than the plate spacing (W

and d in figure II.4). In the actual application described in this thesis, a typical width

was 50mm, and a typical thickness was 800um, or about 1/64th the width. The reason

that this approximation is necessary is that it removes any contributions from fringing

around the outside of the plates [3]. The permittivity ε and permeability µ of the medium

vary depending on what is between the plates. In practice, many times the medium was

air, for which ε (F/m) and µ (H/m) are well known constants. The details of the modes

are discussed in the next section, but it is important to stress that the PPW allows for

propagation of the transverse electromagnetic (TEM or TM$_0$), transverse electric (TE),

and transverse magnetic (TM) modes.
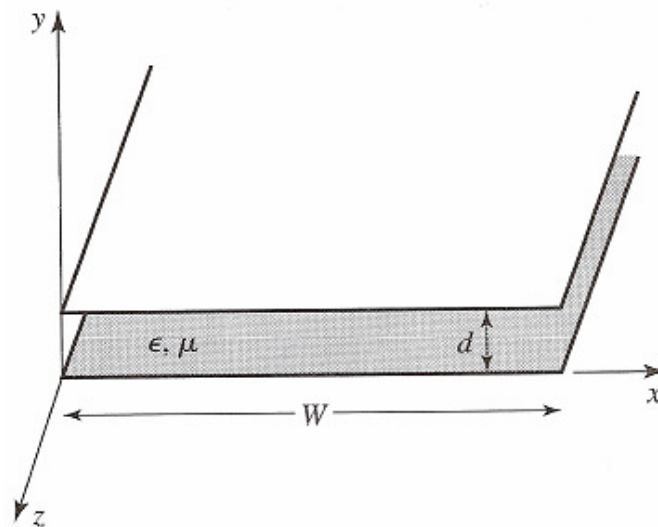
Figure II.4: Basic PPW structure [3]

ii.   Propagation Modes and Cutoffs in a PPW

The two most important modes of propagation for the application discussed in this thesis
are the TEM and TE_1 modes. Unfortunately, higher order modes are usually present
during the measurements with broadband sources, and make usually small, but not
negligible, contributions to the results [6]. For the TEM mode, the electric field through
the PPW as derived using Maxwell's Equations only has a component in the y direction,
and is given as [3]

$$E_y = -\left(\frac{V_o}{d}\right)e^{-j\beta z}$$

 (II.1)

Where V_o is the potential between the plates and β is the phase constant. The magnetic
field only has a component in the x direction and is given as

$$H_x = \left(\frac{V_o}{\eta d}\right)e^{-j\beta z}$$

 (II.2)

Where η is the freespace wave impedance. These equations are accurately represented in
figure II.4 above where the red plot is the electric field and the blue plot is the magnetic
field, and both are perpendicular to each other and the direction of propagation. The

characteristic impedance and phase velocity can be derived from the above terms and are

given respectively as

$$Z = \frac{V}{I} = \frac{\eta d}{w}$$

(II.3)

$$v_p = \frac{\omega}{\beta} = \frac{1}{\sqrt{\mu\varepsilon}}$$

(II.4)

The characteristic impedance is dependent upon the material inside the waveguide (377Ω

for free space) multiplied by the opening height divided by the waveguide width. Using

the assumption mentioned before that W/d is around 1/64, a typical value for the

impedance would be 5.9 ohms, meaning there is a large mismatch between free space and

the waveguide. In equation II.4 above, one can see that for an ideal TEM transmission,

the propagation constant β varies linearly with frequency. This means that the phase

velocity is the same for all frequencies, thus there is no dispersion to worry about. This is

not the case for other propagation modes however.

For the TM modes, the electric field components are derived as

$$E_x = 0$$

(II.5)

$$E_y = -\frac{j\beta}{k_c}A_n \cos\left(\frac{n\pi y}{d}\right)e^{-j\beta z}$$

(II.6)

$$E_z = A_n \sin\left(\frac{n\pi y}{d}\right)e^{-j\beta z}$$

(II.7)

While the magnetic field components are

$$H_x = \left(\frac{j\omega\epsilon}{k_c}\right)A_n \cos\left(\frac{n\pi y}{d}\right)e^{-j\beta z}$$

(II.8)

$$H_y = 0$$

(II.9)

$$H_z = 0$$

(II.10)

As can be seen, for a mode number of 0, the sin term for the electric field is 0 and the cosine term in the magnetic field is 1, making the fields identical to TEM mode. For the TE modes, the electric field components are

$$E_x = \left(\frac{j\omega\mu}{k_c}\right)B_n \sin\left(\frac{n\pi y}{d}\right)e^{-j\beta z}$$

(II.11)

$$E_y = 0$$

(II.12)

(II.13)
$$E_z = 0$$

And the magnetic field components are

(II.14)
$$H_x = 0$$

(II.15)
$$H_y = \left(\frac{j\beta}{k_c} \right) B_n sin\left(\frac{n\pi y}{d} \right) e^{-j\beta z}$$

(II.16)
$$H_z = B_n cos\left(\frac{n\pi y}{d} \right) e^{-j\beta z}$$

In each of the above TE and TM mode equations, the n refers to the mode number which is 0, 1, 2, 3, etc. The propagation constant for TE and TM modes is given in equation II.17. In order for β to remain a real number in equation II.17, k (the wave number) must be greater than k_c, which is why there is a frequency cutoff for lower frequencies.

(II.17)
$$\beta = \sqrt{k^2 - k_c^2}$$

Where

(II.18)
$$k_c = \frac{n\pi}{d}$$

Equations II.17 and II.18 can be expanded to show that the propagation constant does not vary linearly with frequency. This expansion is given in equation II.19.

$$\beta = \sqrt{(\omega\sqrt{\mu\epsilon})^2 - \left(\frac{n\pi}{d}\right)^2}$$

(II.19)

This means that the phase velocity, given in equation II.20, will be different for all

frequencies creating dispersion. This dispersion is evident in figure II.5 for the TE_1

propagation, as the lower frequencies take longer to propagate through the waveguide.

$$v_p = \frac{\omega}{\beta}$$

(II.20)

The group velocity for TE and TM modes is calculated by taking the inverse of the

derivative of the propagation constant with respect to frequency, and is shown in equation

II.21.

$$v_g = \left(\frac{d}{d\omega}\beta\right)^{-1} = c\frac{\beta}{k_o}$$

(II.21)

In general, higher order modes are not desirable in the waveguide, as they end up

distorting time-domain signals due to different phase delays [6] as well as potentially

introducing additional losses. An important number then is the cutoff frequency for each

mode. The higher the frequency, the more modes propagate, thus the cutoff frequency

should increase as n increases. The cutoff for both TE and TM modes is given in

equation II.22.

$$f_c = \frac{n}{2d\sqrt{\mu\epsilon}}$$

(II.22)

As one can see, the cutoff is also a function of the opening height d and the medium

between the plates. One important thing to take away from the above equation is that the

spacing between the plates should be as small as possible to prevent higher modes from

propagating in the waveguide. Table II.1 shows the theoretical cutoff frequency for 3

different opening heights across nine modes. This means that, for example, when the

opening is larger than 1mm and we utilize the full 2 THz bandwidth of the Picometrix

system we may have to consider more than 10 different modes.

Table II.1: TE/TM mode cutoff frequencies vs. opening heights

Mode Number	fc 0.5mm (THz)	fc 0.75mm (THz)	fc 1mm (THz)
1	0.3	0.2	0.15
2	0.6	0.4	0.3
3	0.9	0.6	0.45
4	1.2	0.8	0.6
5	1.5	1	0.75
6	1.8	1.2	0.9
7	2.1	1.4	1.05
8	2.4	1.6	1.2
9	2.7	1.8	1.35

TEM and TE_1 modes both have their benefits and drawbacks in the PPW THz-TDS application [4]. TE_1 mode is very good for measuring details perpendicular to the direction of travel (such as notches), but it suffers from a low-frequency cutoff. TEM mode works well at low frequencies and transmits more power through the waveguide, but it is not sensitive to the before-mentioned grooves or resonator structures [4]. In practice, TEM mode is selected by having the slit of the waveguide oriented perpendicular to the mounting holes on the bottom of the Picometrix transmit and receive heads, and TE_1 mode is selected by rotating either the transmit and receive heads 90° or the waveguide 90°. Figures II.5 and II.6 are a sample of time domain and frequency domain plots of the TE_1 and TEM modes with 0.8mm spacing. As expected from the above analysis, the TE_1 mode cutoff is right around 0.2THz. Additionally, there appears to be some other things happening in the plot of figure II.5, as evidenced by rippling in the TEM mode for later times. This may indeed be a result of higher order TM modes propagating.
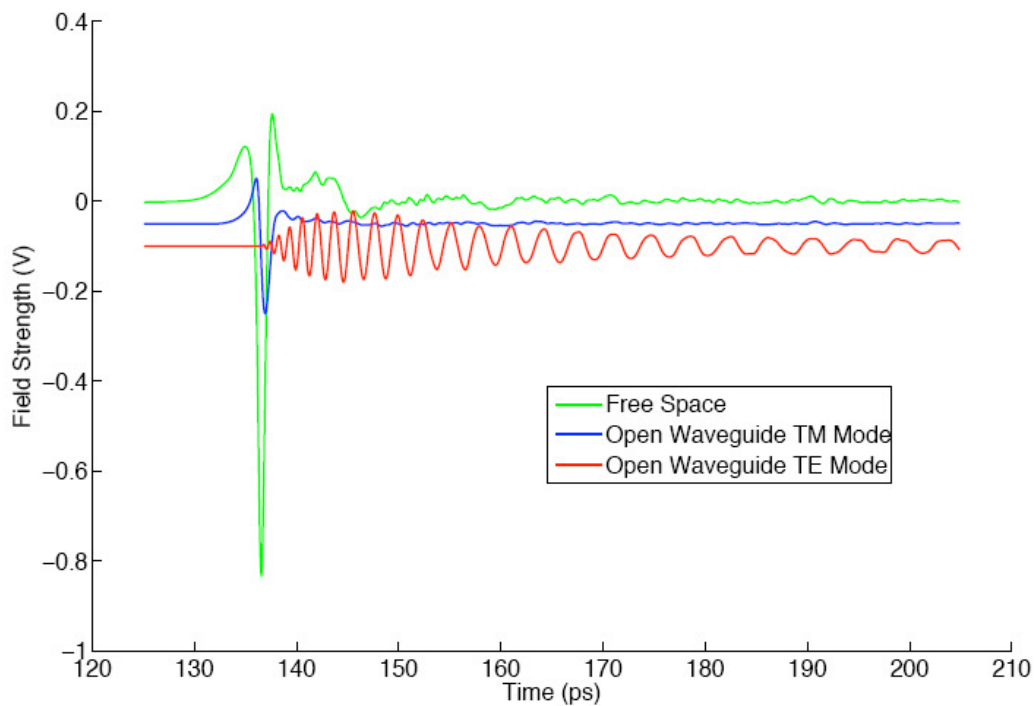
Figure II.5: THZ-TDS comparison plot of TEM and TE PPW propagation
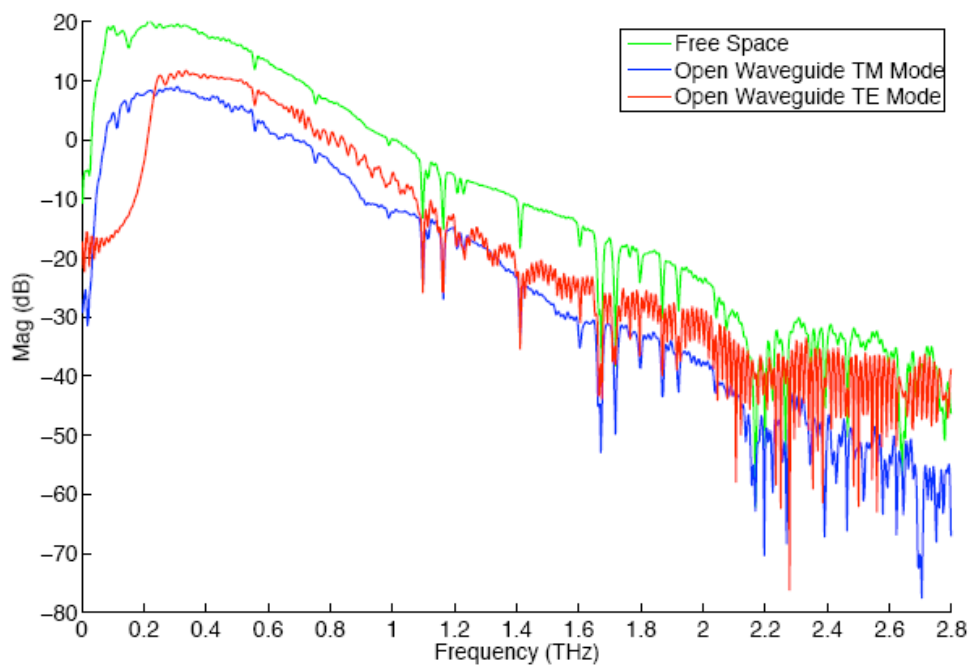
Figure II.6: Frequency domain of figure II.5

iii.   Antenna Structures on Waveguides

An antenna structure could be used to further guide the incoming radiation onto the input of a waveguide. An example of this would be a horn positioned at the input as shown in figure II.6. At the end of the horn, the waveguide begins. The same method could be applied to the output if necessary to increase the amount of radiation the receiver gets.
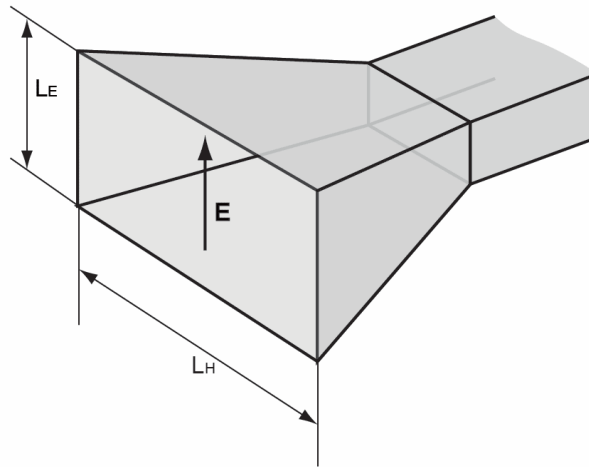
Figure II.7: Horn on the input of a waveguide [3]

Another option would be to use a conical structure to couple the radiation into the PPW. In both cases, the angle of the opening is extremely important (as detailed in figure II.8), and varies with the frequency range desired. Any conical or horn transition needs to be many wavelengths long in order to achieve good directivity [7], but this is not a problem when working in the THz range, as the wavelengths are very small (less than 1mm). Figure II.8 is a picture of such a conical structure used in a measurement covered by this thesis.
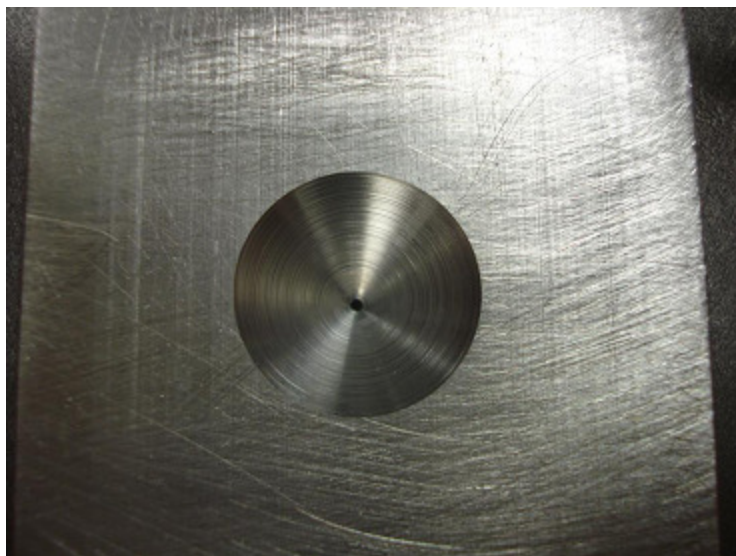
Figure II.8: Machined horn used at input of PPW
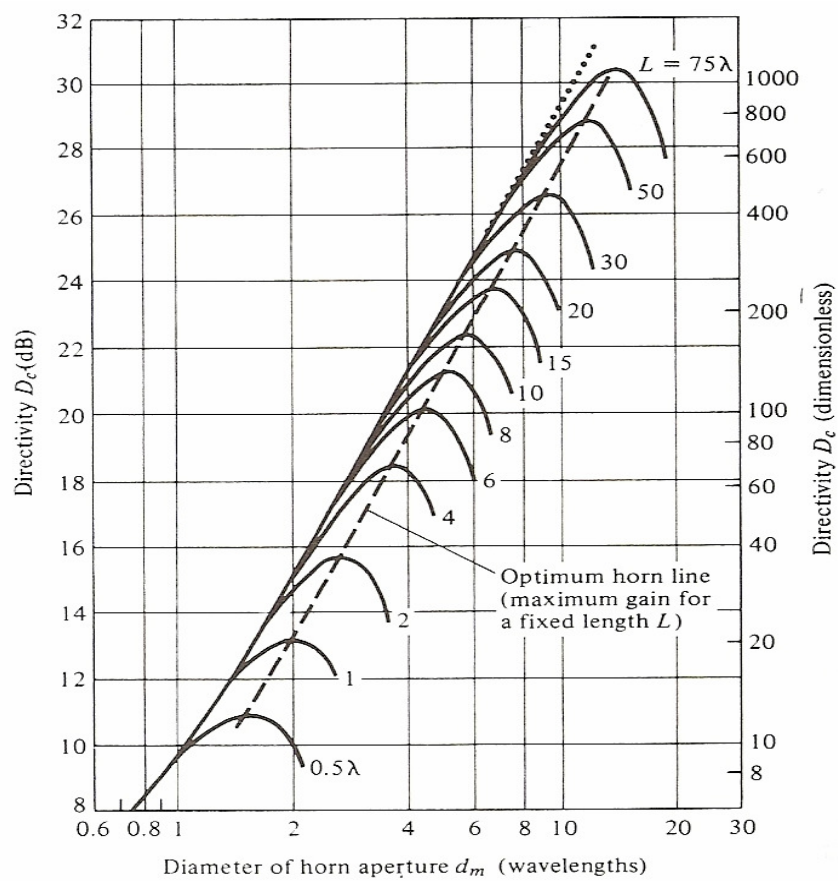
Figure II.9: Horn diameter vs. directivity [7]

D.   Optical Lenses in THz Research

An optical lens can be used to focus terahertz energy onto the opening of a waveguide to help direct more power into the input, as well as focus energy coming out of the waveguide to receive more power. A problem with using optical lenses is that their focusing ability is frequency dependant. Additionally, many typical lens materials (such as glass), have extremely high attenuation properties in the THz region. In practice however, lenses made of high-resistivity silicon [1][2] and high-density polyethylene (HDPE) have been used with good results. These lenses can be expensive to make or purchase, but they can be used on almost any fixture, and thus are more flexible than having an antenna structure machined for each waveguide. Lenses were used during the course of this thesis, and they were plano-convex in shape. Figure II.10 is the general shape of a plano-convex lens where the collimating entering radiation (shown as blue lines) is focused to a point.
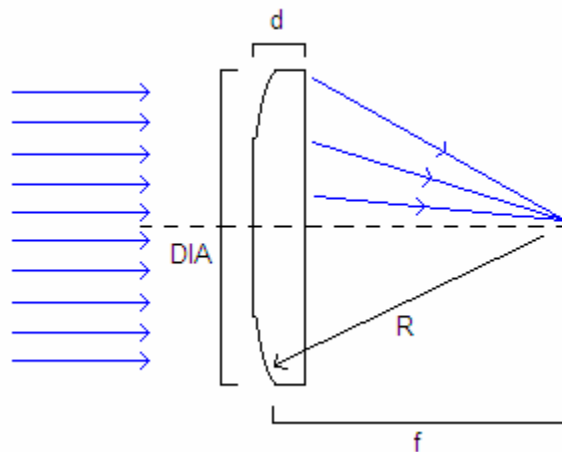
Figure II.10: Plano-convex lens

The most important terms in the above figure are f (focal length), DIA (diameter), d (lens thickness), and R (curvature radius of curved side). When designing a lens, the equation below is used, which is also known as the lensmakers equation.

(II.23)
$$\frac{1}{f} = (n - 1)\left[\frac{1}{R_1} - \frac{1}{R_2} + \frac{(n-1)d}{nR_1R_2} \right]$$

Where R_1 is the radius of curvature on the signal source side (R in figure II.10), and R_2 is the radius on the output side (∞ in this case). The important thing to remember in the above equation is that the index of refraction, n, is frequency dependant for any given material. For a material chosen for a particular frequency range, the refractive index will not change too much, but it will still have subtle effects on the focusing ability of the lens. Designing optical lenses was beyond the scope of this research, so in practice lenses designed for the Picometrix transmit and receive heads were used.

III.   Waveguide Designs, Manufacturing, and Experimental Setups

This section describes the methods used to determine the most optimal shape of the

waveguide. A variety of experiments were carried out to determine the structure of a

flexible fixture that was developed for future work. The system used for all

measurements was the Picometrix T-Ray 4000 with transmitting and receiving lenses. A

variety of different setups were used to hold the PPW steady in the middle. Figure III.1

is a picture of a general setup.
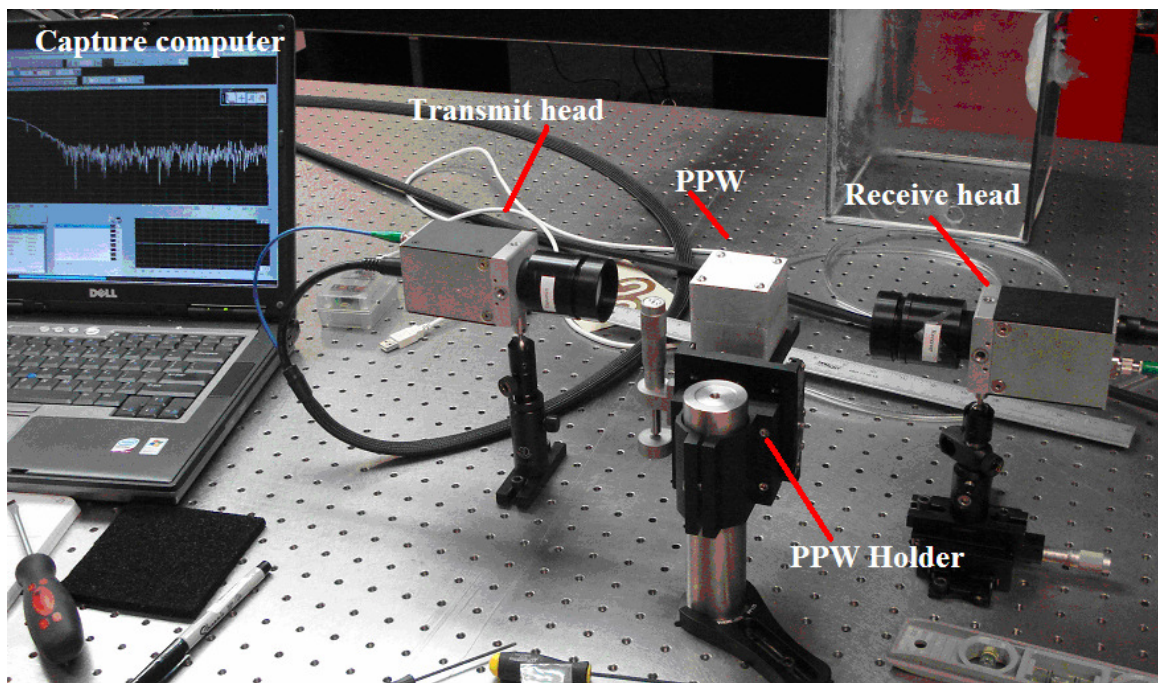
Figure III.1: Basic PPW transmission in TEM mode

Initially, a proof of concept fixture was developed as a starting point for the later

experiments. The plates that made up the top and bottom of the PPW were 25mm (1

inch) tall by 50mm (2 inches) wide by 50mm long, and the spacing between the plates

was around 1mm. Data was collected showing that when the plates were aligned parallel

to the optics table, the primary propagation was in TE$_1$ mode. The easiest way to tell this

from the data was to look at the frequency-domain plots. A low-frequency cutoff

indicates a TE$_1$ mode transmission, because the cutoff is determined by the equation

mentioned before

$$f_c = \frac{n}{2d\sqrt{\mu\epsilon}}$$

(III.1)

Where n is 1, and d is the spacing between the plates. The TEM mode has no low-

frequency cutoff but there is no transmission at very low-frequency due to the low-

frequency cutoff of the Picometrix system.

 Rotating the plates by 90° changed the primary transmission mode to TEM. The amount

of attenuation through the waveguide was around 10dB, and it was almost constant over

the frequency range. A picture of the generic setup is shown in figure III.2. The

difference from figure III.1, however, is that the transmit and receive heads are rotated by

90°, achieving the same effect as rotating the PPW.
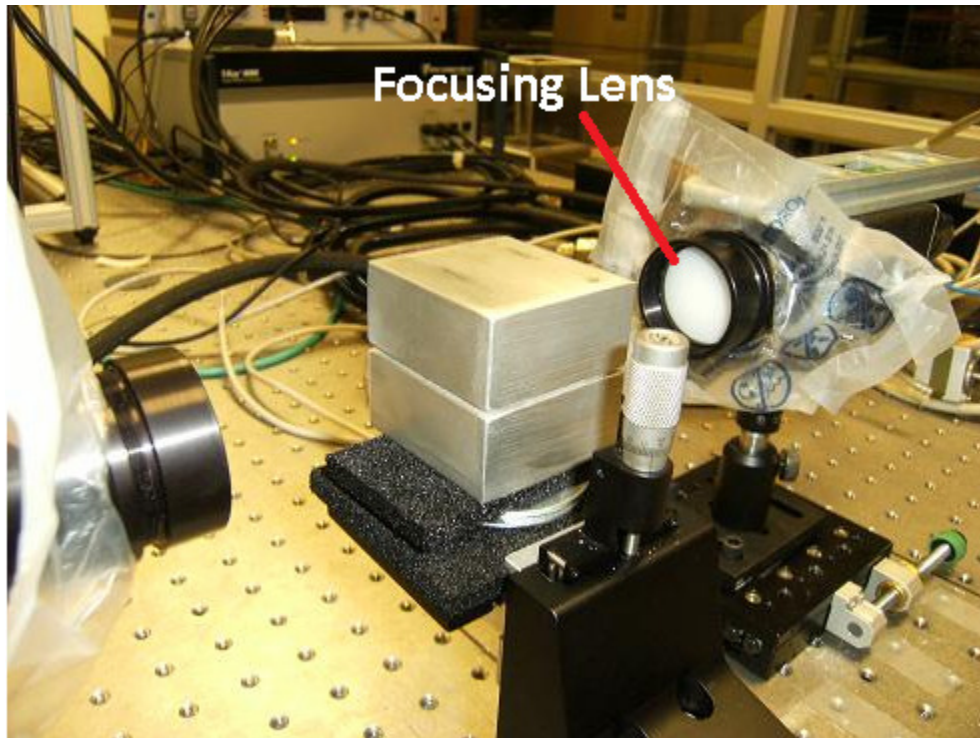
Figure III.2: Basic setup for PPW transmission in TE_1 Mode

The transmission mode of the above photo would be TE_1 because the waveguide slit is parallel to the bottom mounting holes of the transmit and receive heads. The above setup, while simple, yielded some very useful data, and was a good starting point for future measurements.

A.   Using Lenses

In order to focus the THz energy from the large area produced by the collimating lenses (which have a beam width of around 1.5 inches in diameter) down to a smaller point, lenses were acquired from Picometrix with focal lengths of 1 one inch, 3 inches and 6

inches[8]. These lenses are normally mounted inside of the transmit and receive heads.

Data was taken with all three of these lenses and compared against the normal

collimating lenses. It was found that using 3-inch lenses on both the input and output

heads and keeping the heads 7 inches apart provided the best results in both received

power, and repeatability of measurements. It would seem that the ideal distance would

be 8 inches, the extra 2 inches coming from the length of the PPW, but experimentation

proved this not to be the case. All future experiments were performed with the 3-inch

lenses kept 7 inches apart. The 6-inch lenses do focus the THz better than the collimating

lenses, but the 3-inch lenses offer better performance, as they focus it into a smaller area.

The 1-inch focal length lenses ended up being too sensitive to alignment. Figure III.3 is a

picture of the 1-inch lenses attached to a PPW (this setup was used for a different

experiment on another system). The radius of curvature increases as the focal length

decreases, so the 3-inch lenses were about half as thick. The 3-inch lenses can be seen

included in the receive head in figure III.2 above.

---

[8] For brevity, these are referred to as 1-inch, 3-inch and 6-inch lenses, indicating their focal length.
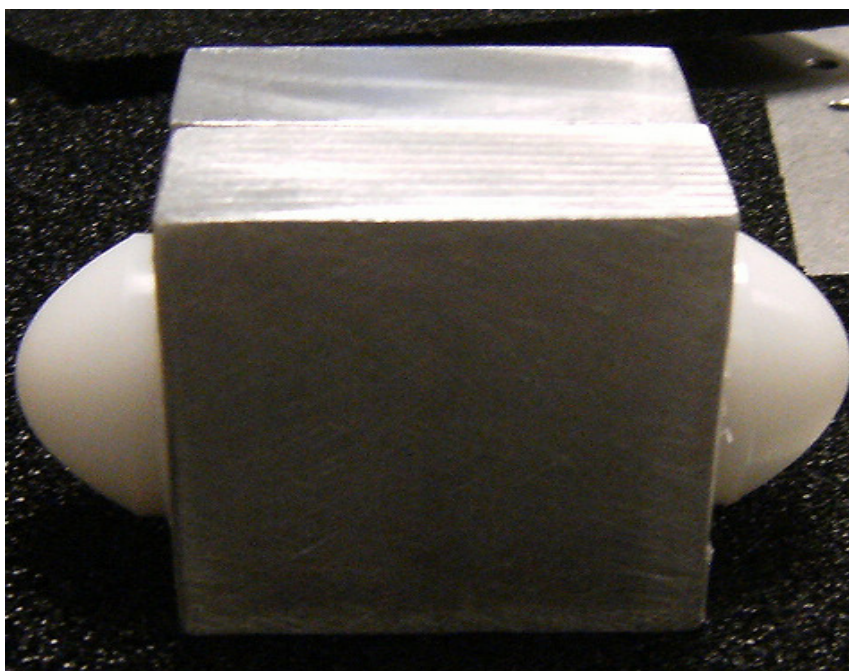
Figure III.3: Focusing lens attached to PPW

While the setup of figure III.3 was not used in any experiments, it shows how the system

works with the lenses which are mounted directly to the PPW. Collimated THz radiation

from the Picometrix system shines on the convex side of a lens[9] (usually contained within

the transmit/receive heads of the Picometrix). The lens focuses the radiation down to a

small point at the input of the waveguide. The radiation propagates through the

waveguide and strikes the planar side of the second lens on the far side. This lens

collimates the radiation which travels to the receive head of the Picometrix. This type of

setup appears to be most commonly used by groups involved in THz research.

---

[9] These lenses are usually mounted within the transmit/receive heads of the Picometrix.

B.   Transmission vs. Opening Height

Another important characteristic of the PPW is the amount of attenuation present as the

spacing between the waveguide plates is increased or decreased. Additionally, the low

frequency cutoff when transmitting in TE mode is affected by the spacing. Initially, the

method used to set the spacing was sliding in machinist feeler gages on either side of the

waveguide. Sheets of 800um thick high-density polyethylene plastic (HDPE) cut into

strips were also used. The advantage of using HDPE was that it is nearly transparent in

the THz spectrum, reducing the concern for possible reflection off the sides inside the

waveguide. The final solution for setting the height was to use high precision machinist

spacers on the flexible fixture. Figure III.4 is a close-up of the spacing between the plates

with the feeler gages between them. For most data, waveguide spacing of around 0.6mm

to 1mm were used.

For any future application, (for instance, characterizing a specific material inside of a

PPW) data at several thicknesses should be taken. This is because there is usually an

ideal thickness for which a good amount of radiation propagates through the waveguide,

but where higher TE/TM modes do not begin to have a noticeable effect on the data.
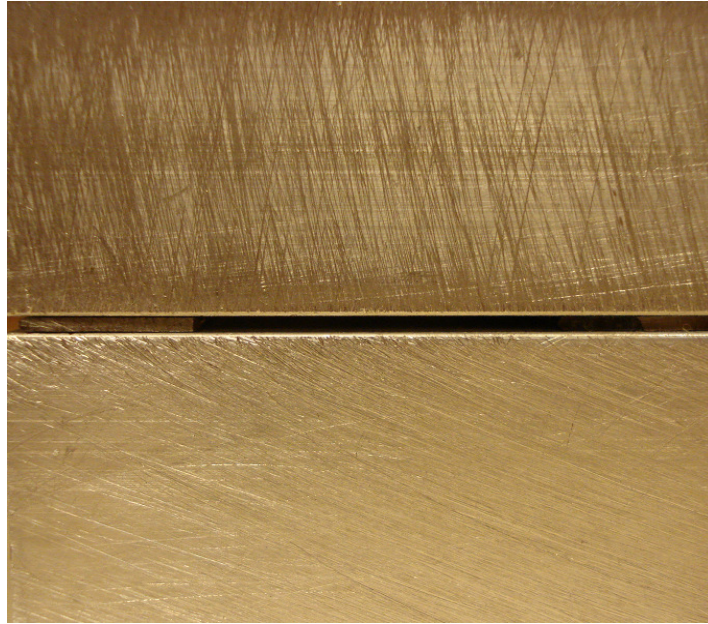
Figure III.4: Close up of waveguide opening

C.   Waveguide Length

One factor to consider along with the height of the opening is the length of the waveguide. One would expect that as the length of the waveguide was increased, greater attenuation would be observed. In an attempt to characterize this, three different lengths of waveguide were built and measured. Besides the normal 50mm long waveguide, waveguides of 25mm and 12.5mm in length were measured and compared to each other. Because 50mm covers many wavelengths[10] this was consider sufficient to avoid any transitional effects at input and output. A longer waveguide was not considered practical for further research due to excessive length and losses.

---

[10] Recall that free-space wavelength at 300 GHz is 1mm.

D.   Surface Polish

Another important factor to consider is how sensitive the waveguide attenuation is with respect to surface roughness. To check this, a relatively rough surface (polished with 60-grit sandpaper) was compared to a mirror-smooth finish (polished with 600-grit sandpaper). A close-up of the two polishes is shown in figure III.5 One must be careful when using highly-polished surfaces as they can easily be scratched, especially when using soft metals such as aluminum. Each individual particle on 60-grit sandpaper has a diameter of around 265μm[11], which is very close in size to the wavelengths being used. While the width of channels cut into the block may be this wide, the depth of the channels is dependent upon the pressure being used while polishing, and actually much less than a wavelength.

Figure III.5: Close up of polished waveguide surfaces

---

[11] As characterized by the Coated Abrasives Manufacturers Institute

E.   Gold plating of PPW

Another consideration on the design of the waveguide was the materials of which it is constructed. Aluminum was chosen because of its low price, its ease of machining, and its conductive properties. One other material that was tried however was gold. Aluminum plates (polished with 600-grit sandpaper) were coated with an extremely thin (<<1µm) coating of gold by the Portland State University physics department and compared against normal aluminum plates. Methods of depositing a thicker layer of gold onto the waveguide blocks were not available at the time, but it was hoped that a thin layer would give an idea of how much improvement we could expect. Upon further analysis, it was determined that the layer of gold was not thick enough to ensure that the THz radiation does not penetrate into the aluminum.

F.   Different Opening Shapes

One area that was studied extensively was the shape at the input and output of the waveguide. The idea was that it may be possible to couple in and focus more signal power through the use of different structures at the input. Lenses (in addition to the transmit and receive lenses mentioned above) were considered for this initially, but the fabrication price, complexity, and frequency dependence issues weight heavily against this idea, and it was not pursued further. An angled waveguide of about 45 degrees opening angle was originally tried, followed by several cone structures. The first cone

structure was a funnel-shape of 90° drilled directly into the front surface of the

waveguide, so it was actually half a funnel on the top and half on the bottom waveguide

plates with a break in between for the waveguide opening. The next type was on a

separate plate attached to the front of a normal waveguide. Neither of these structures

were found to be very successful in increasing power in either TE or TEM modes. With

further research it was found that any angle at the input and output would need to be

much smaller than 45° (in the neighborhood of 15 degrees), and the efficiency of the

structure drops off quickly once you are out of the optimum opening angle range [7].

However, our options were limited due to use of countersink bits in manufacturing as

these bits normally have angles in excess of 45°. Some pictures of the setups created are

shown in the figures III.7, III.8, and III.9.
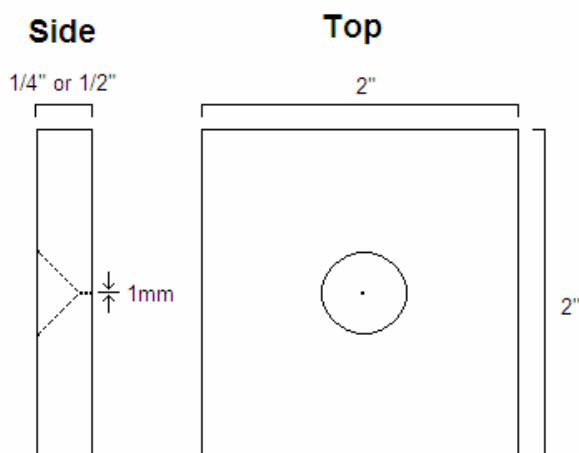
Figure III.6: Drawing of conical plate used for attachment to front or back of PPW
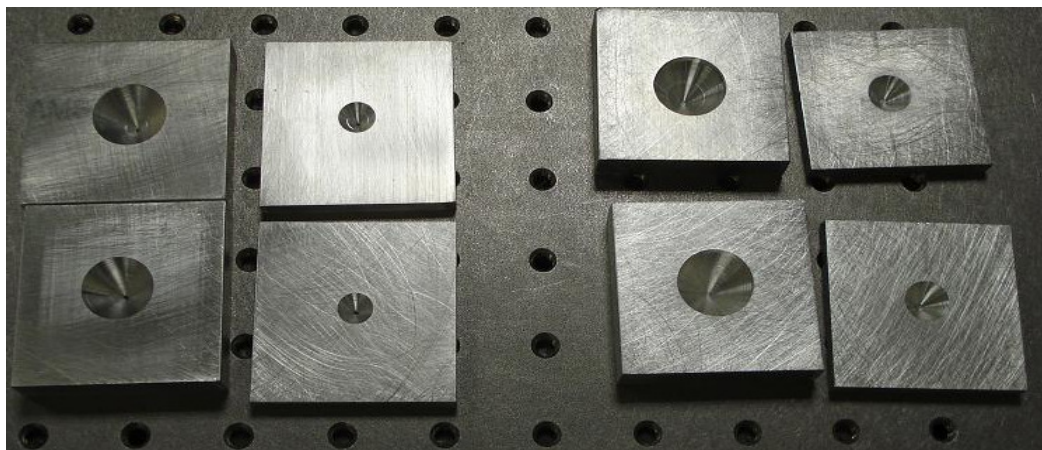
Figure III.7: Photograph of different conical plates used

Figure III.8: PPW side of conical plates in figure III.7 with input/output hole marked
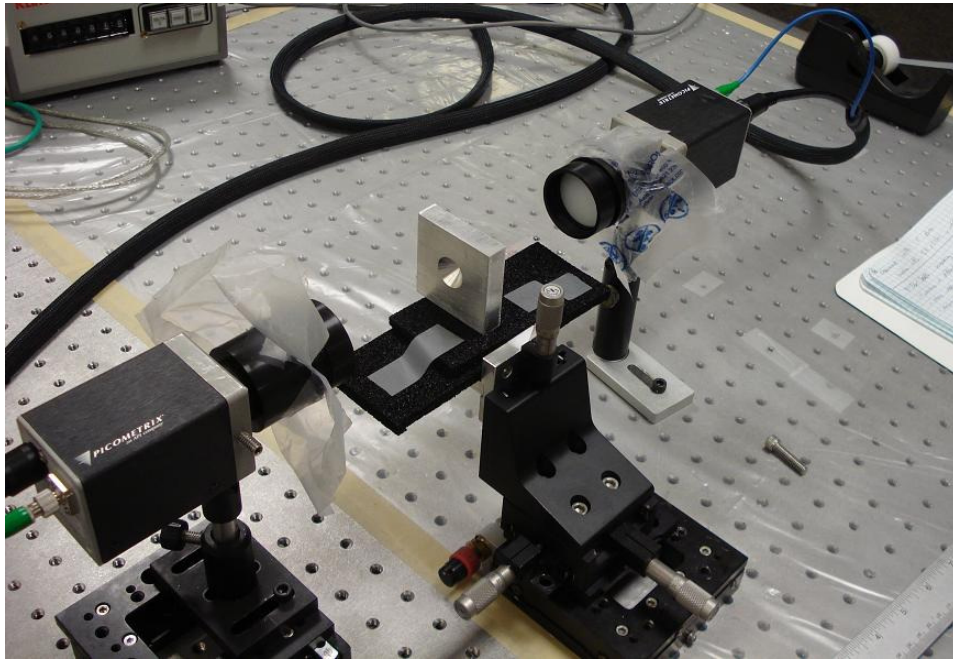
Figure III.9: Setup used to measure conical plate by itself

G.   Flexible Fixture

Once all the possible waveguide variations were investigated, a permanent flexible

fixture was built and tested. The benefits of this fixture are that it is cheap to make,

easily reproducible, performs very repeatable measurements, and can be adjusted for

different opening heights quickly. Several fixtures were made, using both 1 inch and ½

inch thick plates. The plates are all 2 inches wide by 2 inches long, and made of

aluminum. These dimensions were chosen so that the opening height would be much

smaller than the width, and that the transmission distance was many wavelengths. The

thickness of the plates was left large to block out any excess THz radiation from

transmitting above or below the waveguide.   Holes are drilled through the top plate and

halfway into the bottom plate. The bottom plate holes are tapped for #8-32 screws, which screw in through the top plate and sandwich the whole setup together. Finally, precision washers are placed around each screw to set the opening height. Pictures of this setup are shown in figure III.10.
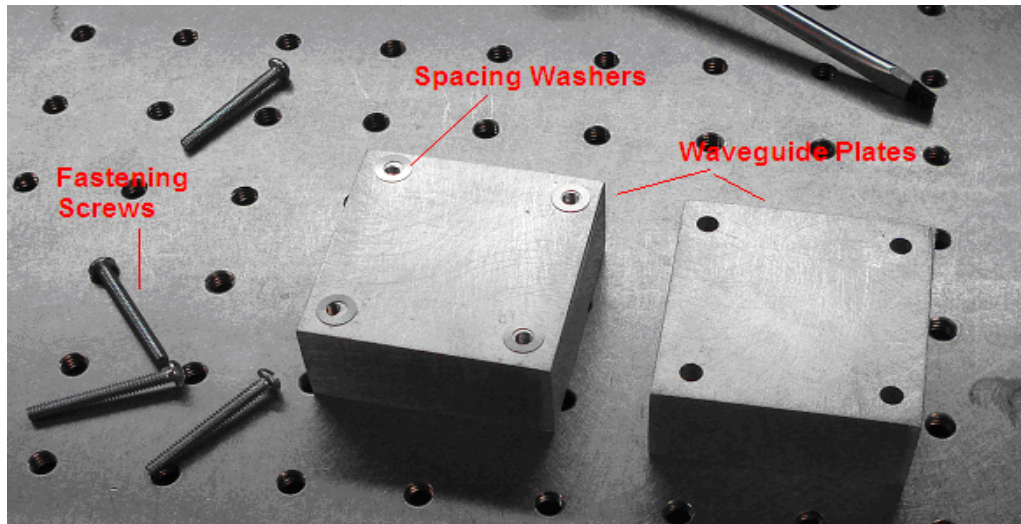
Figure III.10: Flexible PPW fixture components

H.   Resonator Waveguide

The final area of study was testing the effect resonator structures on the surface of the waveguide, with the hopes of producing areas of higher energy in certain parts of the waveguide [9] or to remove specific frequencies. A 381 μm (15mils) wide groove was cut into one of the waveguide plates to a depth of around 381 μm and characterized. Figure III.12 is a drawing of a side view of the groove structure being measured, along with a photograph in figure III.13 of the plate with the groove on it. This was chosen as a

starting point/proof of concept that it could be done. The result of these experiments did

not exactly match up as expected with similar experiments performed by others [4][5], but

some of the data was later verified with simulations.
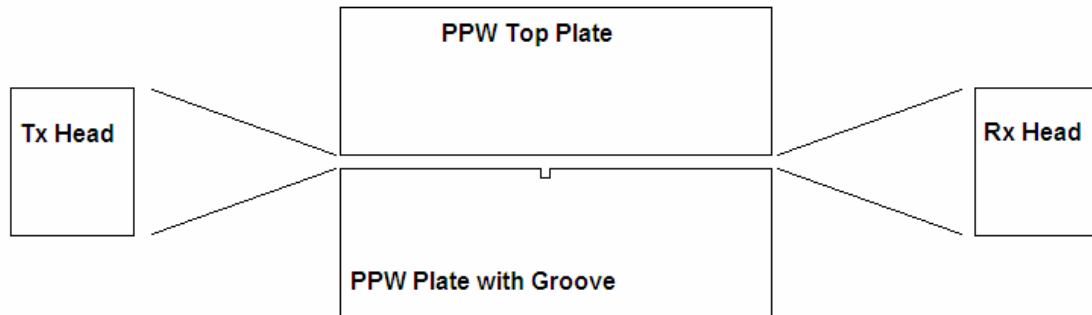
Figure III.11: Side schematic of PPW with groove being measured
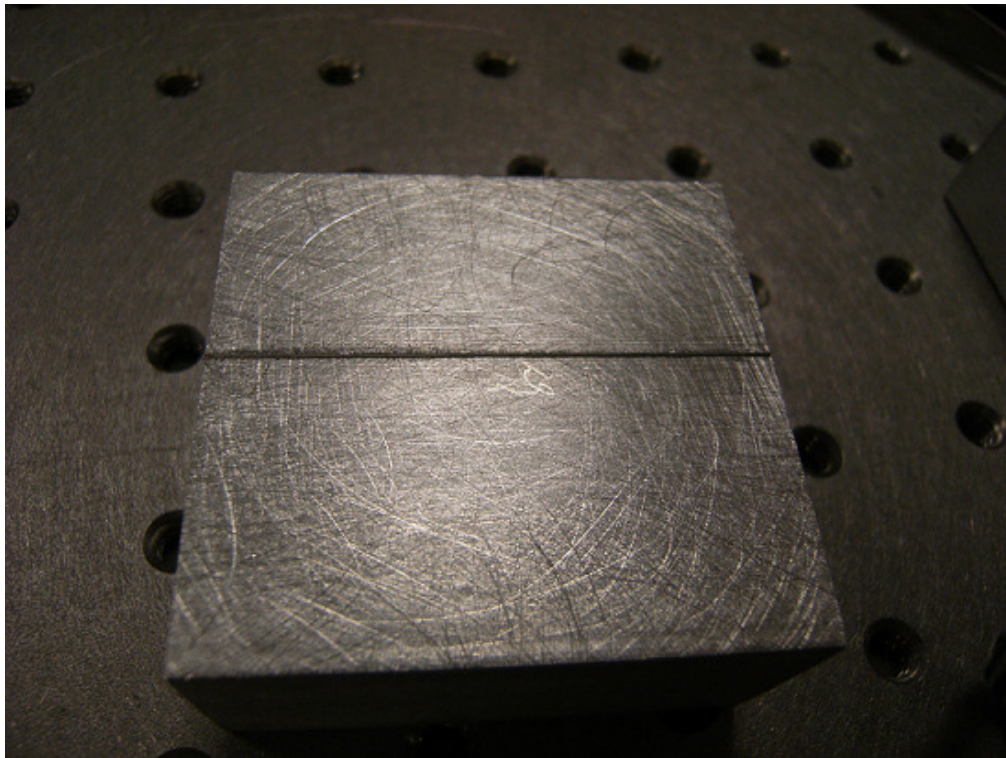
Figure III.12: Photograph of groove on PPW plate

Data was compared to simulations performed in MEEP (MIT Electromagnetic Equation

Propagation[12]), a free finite-difference time-domain simulation software simulator, used

to model electromagnetic systems. The method used by MEEP is actually a continuous-

wave simulation, similar to an S21 measurement taken by a vector network analyzer.

The input frequency was swept from 0.039THz to 1.14THz and the output was calculated

for each frequency. There were also idealities assumed for the simulation, such as a point

source for the THz radiation and an infinitely wide waveguide.

After machining the groove shown in figure III.13 into the waveguide, it was determined

that it was far too difficult to use this as a method of building a resonator, at least with the

tools available in the machine lab at Portland State University. One problem is that

381μm is almost too large of a gap to be used in THz research. Another manufacturing

issue was that at 15mils and smaller, the typical machining bits used to cut the groove

into the waveguide are too delicate to use on aluminum. In order for this to be pursed

further, specialty machine houses would need to be contracted, or a different method to

have a grooved surface (such as a metalized silicon structure [9]) would need to be used.

---

[12] http://ab-initio.mit.edu/wiki/index.php/Meep

IV.   Measurement Results and Discussion

All measurements unless otherwise specified were performed on the Picometrix system with 3-inch focal length lenses 7 inches apart with the waveguide in the center. Averaging of 6000 samples per measurement was used to lower the noise and extend the frequency range. Before the PPW was placed between the transmit and receive heads, the heads were aligned while 7 inches apart until the maximum signal was received. Any misalignment between the heads caused some frequency bands to not be received as well, so this step was very important in order to ensure good results. Additionally, great care was taken to ensure that the front and rear of each waveguide plate were aligned with each other, and that the waveguide was directly in the center of the transmit and receive heads.

A.   Basic PPW Transmission with Lenses

Once the basics of the setup were in working order, the first real set of data taken compared the 3-inch and 6-inch focal length lenses to the standard collimating lenses. The 1-inch focal length lenses did not provide any useful data due to the extreme sensitivity to placement. Figure IV.1 is a plot of 3 different lens setups for both free space (no waveguide present) and with a 2-inch long PPW. Although all data is received in the time domain, it is typically plotted in the frequency domain through the use of an FFT script in MATLAB.

Freespace vs. PPW Transmission With Different Lenses
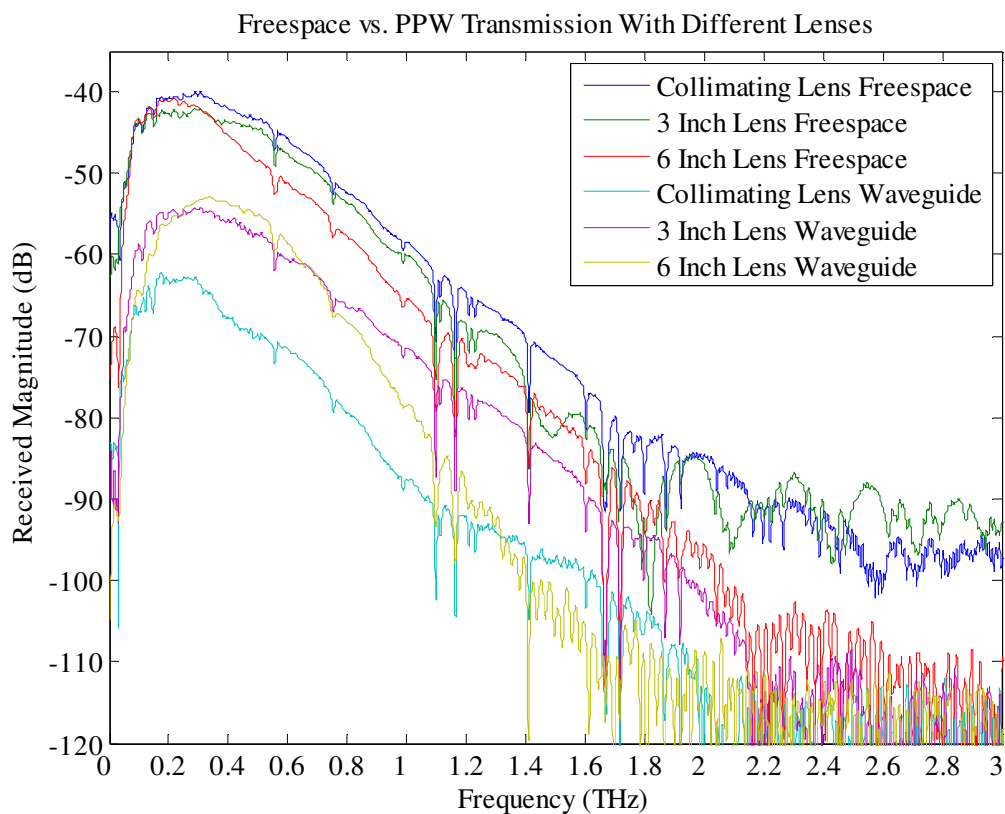
Figure IV.1: Basic PPW transmission plots with lenses compared to free space

As can be observed in the above plot, when transmitting through free space, the collimating lenses perform slightly better than the 3-inch and 6-inch focusing lenses. This is because the collimating lenses are much less sensitive to alignment, and almost all of the transmitted power is received. Additionally as mentioned before, the focusing lenses alignment is frequency dependant. This can be observed by slightly varying the angle of the transmit head to the receive head. When this is done, certain frequency ranges will increase in received power while others may go down.

When transmitting through the waveguide, much more power, around 10dB, is transmitted through with the 3-inch focusing lenses compared to the collimating lenses. This is due to more power being focused at the input and received from the output of the PPW. Compared to the 3-inch lenses, the 6-inch lenses also suffer from higher-frequency drop-off similar to the one observed for the collimating lenses.

As was mentioned previously, the 1-inch lenses were not used due to their sensitivity to alignment. They would theoretically produce a better transmission result than the 3-inch lenses if perfectly aligned at both the input and the output, but because repeatability and ease of use are important factors to consider, the 3-inch lenses appeared to be the best solution. The 3-inch lenses can still be somewhat difficult to align (mostly due to a lack of stable base to hold the transmit/receive heads), but once they are properly aligned the entire setup is very robust and measurements are repeatable. The results of these experiments became the basis for all future measurements.

B.   Transmission vs. Opening Height

Figures IV.2 and IV.3 are plots of transmission versus opening height, one is for TEM mode, and the other for TE_1 mode. As mentioned previously, for this and all future measurements, the 3-inch focusing lenses were used. Table IV.1 shows some discrete values from Figure IV.2 to help further analyze the data.

Waveguide Spacing, TEM Mode
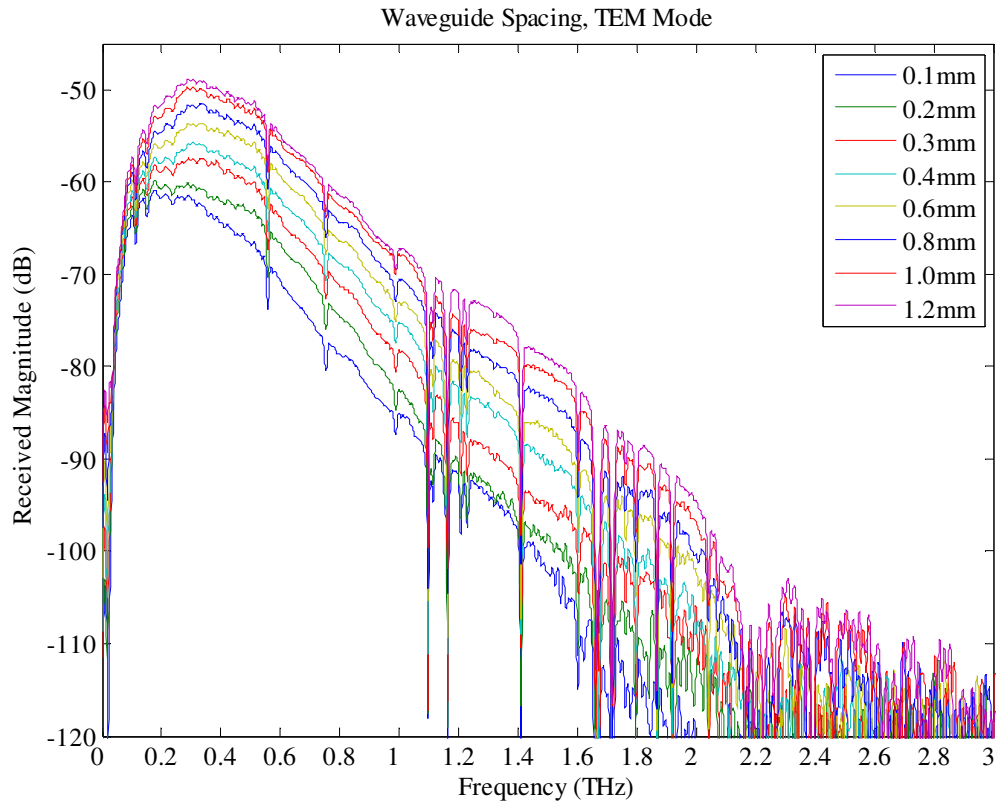
Figure IV.2: Transmitted power vs. opening height, TEM mode

Table IV.1: Received signal magnitude for waveguide different spacings (TEM mode)

	Received signal strength (dB)		
Spacing (mm)	0.5THz	1.0THz	1.5THz
0.1	-66.5	-85.2	-102.2
0.2	-63.2	-82.5	-98.4
0.3	-60.0	-78.3	-95.1
0.4	-58.7	-75.4	-90.4
0.5	-57.0	-74.7	-88.5
0.6	-56.0	-73.1	-86.8
0.7	-55.3	-71.3	-85.1
0.8	-54.2	-70.6	-84.2
0.9	-53.1	-68.4	-83.3
1.0	-52.5	-68.2	-80.7
1.1	-51.9	-67.9	-80.37
1.2	-51.4	-67.2	-79.1

As mentioned previously, the wider the waveguide spacing, the more modes will propagate. For TEM mode transmission, higher order TM modes may propagate if the spacing is too large, thus it is important to find a spacing where there is good transmission without excessive unneeded modes propagating. With this knowledge, a spacing of around 0.8mm seems to be a good choice, as there is a 10-15dB increase in received power going from 0.1mm to 0.8mm, but only a 3-5dB increase going from 0.8mm to 1.2mm. This data also leads to the conclusion that the opening height is linearly related to the received signal power. If we double the height from 0.2 to 0.4mm, 0.4 to 0.8mm, and 0.6 to 1.2mm, the received power increases by around 4.5-5dB in each case.

The signal strength change versus opening height for the TE_1 mode shown in figure IV.3 is closely related to the TEM plot of figure IV.2, but there is the additional complicating factor of the cutoff frequency which limits the lower frequency content. Table IV.2 has the extracted cutoff frequencies from plot IV.3 and the theoretical cutoff frequency.

Waveguide Spacing, TE Mode
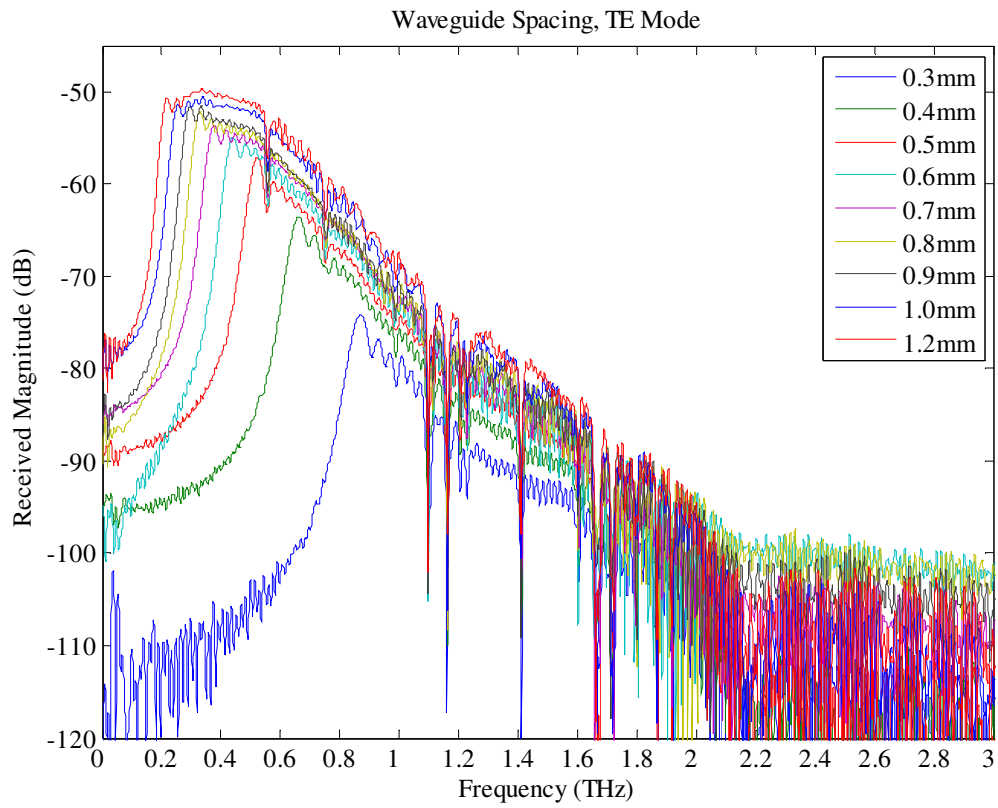
Figure IV.3: Transmitted power vs. opening height, TE mode

Table IV.2: Observed cutoff frequency for different opening heights (TE mode)

Spacing (mm)	Measured Cutoff (THz)	Theoretical Cutoff (THz)
0.3	0.79	0.50
0.4	0.57	0.38
0.5	0.46	0.30
0.6	0.38	0.25
0.7	0.32	0.21
0.8	0.27	0.19
0.9	0.24	0.17
1.0	0.21	0.15
1.1	0.19	0.14
1.2	0.17	0.13

As mentioned before, this relationship is governed by the equation IV.1, where n is the mode number (assumed to be 1 in this case), and d is the opening height.

$$f_c = \frac{n}{2d\sqrt{\mu\epsilon}} = \frac{cn}{2\,d}$$

(IV.1)

For heights of 0.8mm and above, this equation does well in determining the cutoff frequency, but for smaller spacings there appears to be a large amount of error. One cause of this is that the extreme slope of the cutoff lends itself to errors in estimation. The minimum useful spacing seems to be around 0.4-0.5mm, as anything below that has too little received power. As in TEM mode, the ideal opening height is around 0.8mm.

C.   Waveguide Length

The data taken on the 12.5mm, 25mm, and 50mm waveguides is shown in figure IV.2, for both TEM and TE mode with a spacing of 1mm. In the TEM mode plot of figure IV.4, one can see that at low frequency, there is not much change between the 3 lengths, but after about 500GHz, the 50mm plates start to attenuate the signal noticeably more. This could be caused by the focusing lenses focusing higher frequencies to different depths. Because of this, only lower frequencies below 1THz were analyzed. The attenuation for the 50mm PPW can be characterized when the attenuation equation is analyzed. The conductor attenuation is defined as [3]

$$\alpha_c = 8.686\left(\frac{R_S}{\eta d}\right) dB \text{ /m}$$

(IV.2)

Where d is the waveguide spacing height, and R_S is the surface resistivity, which is calculated as

$$R_S = \sqrt{\frac{\omega\mu}{2\sigma}}$$

(IV.3)

From the above equation, one can see that as the frequency ω increases, the surface resistivity increases and thus so does the attenuation.

3 Different PPW Lengths, TEM Mode
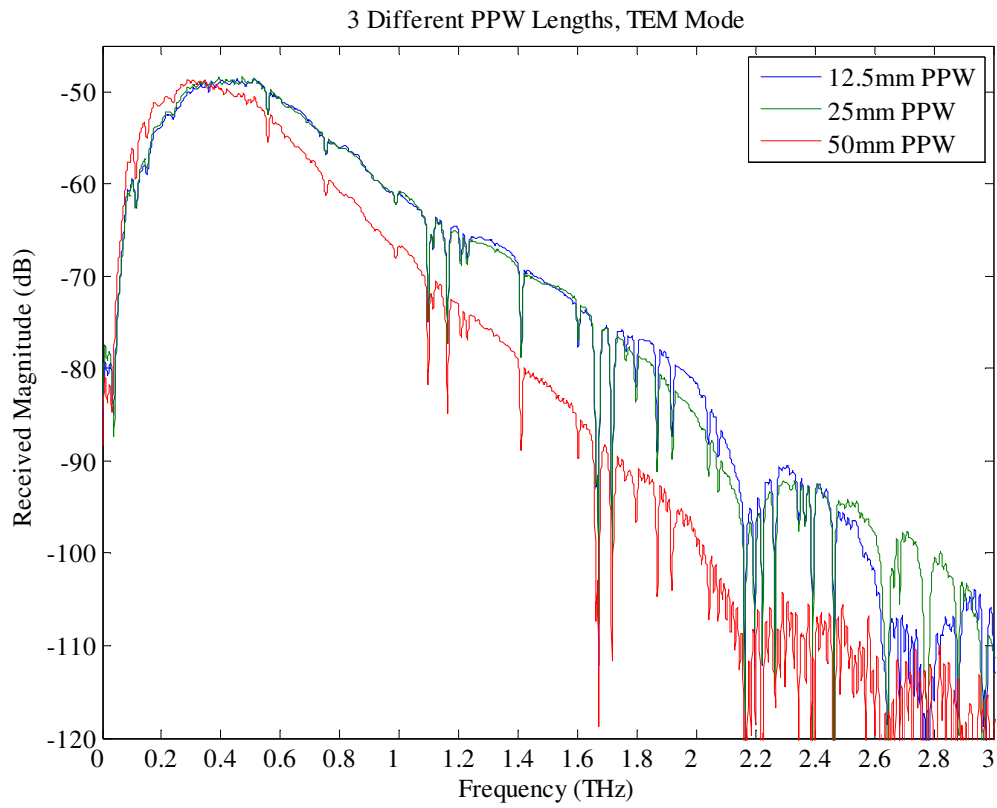
Figure IV.4: Received power for different PPW lengths, TEM mode

The attenuation constant can be estimated by comparing the 25mm waveguide to the
50mm waveguide. The difference between these two waveguides is the attenuation per
25mm. The results of this analysis for several frequencies are given in table IV.3 and
compared against the theoretical values. The measured attenuation values are at least an
order of magnitude larger than expected, and suggest that the dominate cause of
attenuation is caused by some factor other than simple conduction loss

Table IV.3: Extracted and calculated attenuation constants, TEM mode

Frequency (THz)	Measured Att. (dB)	Calculated Att. (dB)
0.5	1.788	0.131
0.6	2.709	0.143
0.7	3.332	0.155
0.8	4.057	0.166
0.9	4.300	0.176
1.0	4.348	0.185

The results for the TE mode measurements are given in figure IV.5 and are similar to

those of figure IV.4. The attenuation values from figure IV.5 were extracted into table

IV.4, and are very similar to those of table IV.3. The theoretical attenuation for a TE

mode is

$$\alpha_c \ = \ 8.686 \left(\frac{2 \left(\frac{n\pi}{d} \right)^2 R_S}{k \eta \beta d} \right) \ dB \text{ /m}$$

(IV.4)

Where n is the mode number, which is 1 in this case, and k is the wave number. The

equation is proportional to

$$\alpha_c \ \propto \ \frac{\sqrt{\omega}}{\omega}$$

(IV.5)

This should make the higher frequencies attenuate less than the lower frequencies, and as

one can notice in table IV.4, the attenuation increases with frequency contrary to

expected. Once again, this points to the fact that the attenuation is being caused by

another factor.
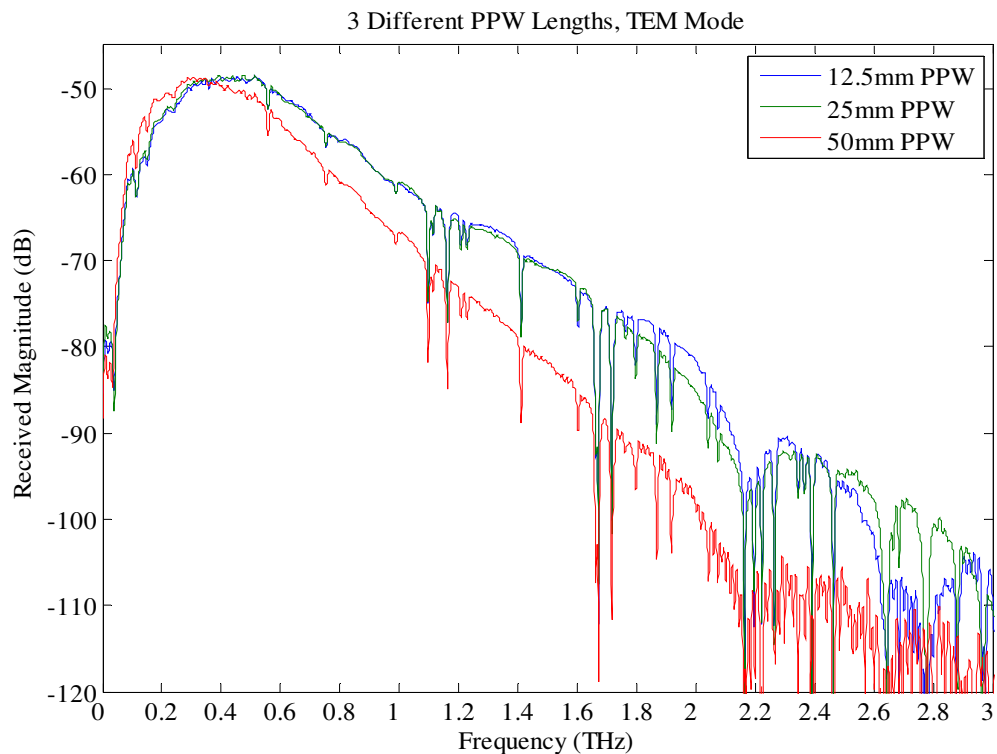
Figure IV.5: Received power for different PPW lengths, TEM mode

Table IV.4: Extracted attenuation constants, TE mode

Frequency (THz)	Measured Att. (dB)	Calculated Att. (dB)
0.5	0.9078	0.024
0.6	2.039	0.018
0.7	1.887	0.014
0.8	4.511	0.012
0.9	3.987	0.010
1.0	4.907	0.008

D.   Surface Polish and Gold Plating

The results comparing different surface polishes were combined with the gold-plated

waveguide results due to the similarity of their subject matter. As can be observed in the

figures IV.6 and IV.7, there is a 1-2dB advantage to using 600-grit to polish over 60-grit,

especially at higher frequency. This would be expected as the grooves cut into the

surface of the waveguide by the sandpaper (around 265μm as stated previously) are on

the same order as the size of a wavelength, and can cause some scattering. As the

frequency increases and the wavelength decreases in size, one would expect the 600-grit

polished blocks to perform better.
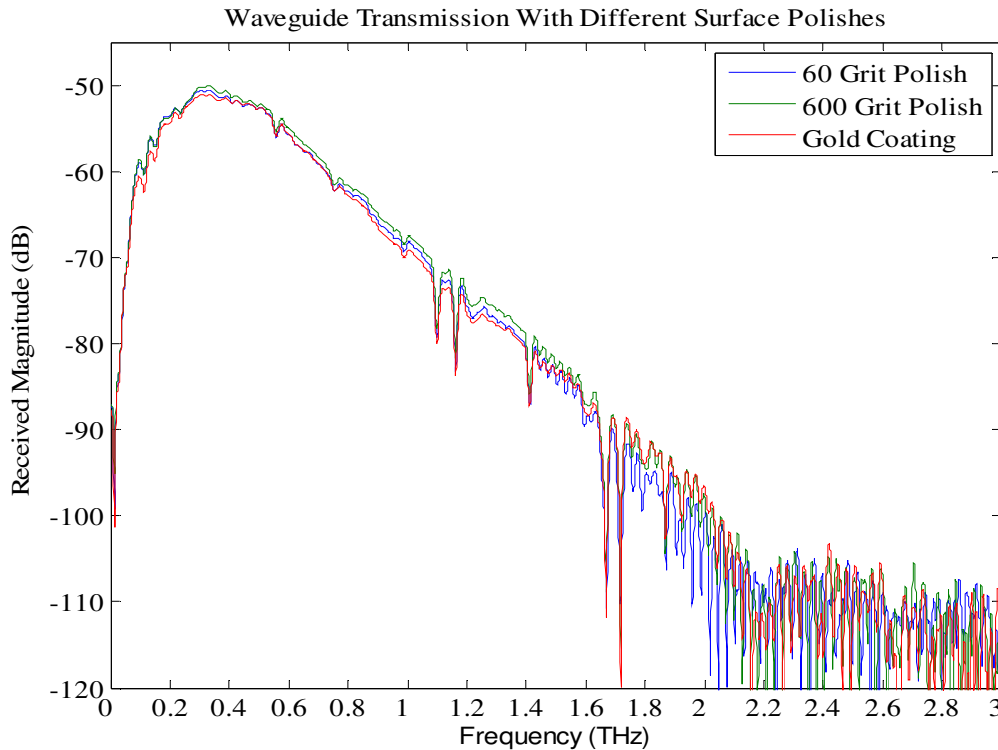
Figure IV.6: Surface polish and gold plating, TEM mode

The gold plating was about 1dB lower in transmission than the 60-grit polish. Figure

IV.7 shows a close-up of the data.
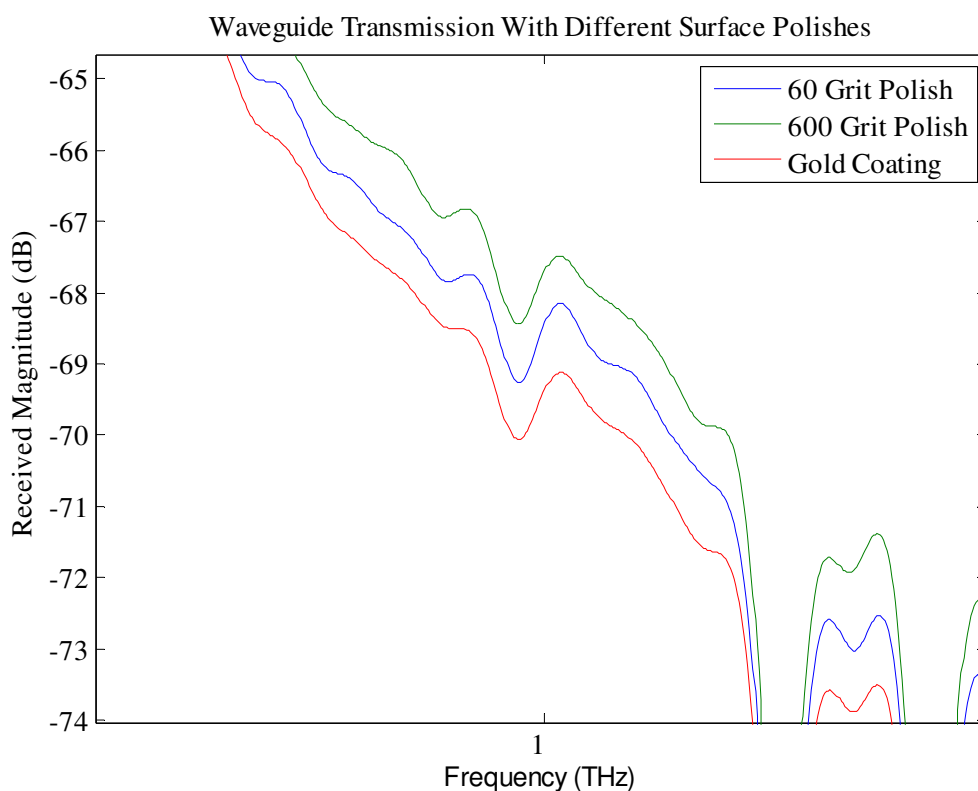
Figure IV.7: Close-up of figure IV.6 at 1THz

This was slightly surprising, as gold would have been expected to be as good as or better

than aluminum. It is possible that the very thin layer of gold deposited on the aluminum

surface was in fact too thin, so an area of future study would be to take data with a thicker

deposition of gold. As mentioned before, the layer of gold was very thin. So thin in fact

that the color was a grayish gold, meaning that you could see the aluminum through parts

of it. The skin depth, the depth where the amplitude fields decay by 1/e in a conductor,

is

$$\delta_s = \sqrt{\frac{2}{\omega\mu\sigma}}$$

(IV.6)

In equation IV.6, σ is the conductivity of the material. The conductivities for several

useful waveguide materials are given in table IV.5

Table IV.5: Material conductivities[13]

	Conductivity at 20°C (10⁷S/m)
Aluminum	3.816
Copper	5.813
Gold	4.098

A calculation of the skin depth at 1THz for gold gives 78.6nm, and it is very probable

that the gold deposited on the PPW plates was thinner than that. A good thickness of

150-250nm would possibly yield better results.

The conclusion that can be drawn from this data is that it is a worthwhile endeavor to

make sure the parallel plate waveguide surfaces are well-polished with no scratches or

other surface abnormalities.

---

[13] Taken from appendix of [3]

E.   Different Opening Shapes

The first opening shapes tested were the half-conical structures drilled directly into the front of the waveguide. A variety of combinations were tried, including analyzing with a horn only on the input, only on the output, and both on the input and output. These results were also compared against having a 45° edge at the input of each waveguide plate (for a total of 90° opening angle). The results for these experiments are shown in figure IV.8. For all measurements, the 3-inch lenses were used. As can be noticed, there is not much benefit to any of these schemes. In the TEM mode plots of figure IV.8 for example, there is only a small difference between the plots. There are some differences in the 1.3-2THz range, but these are differences of several dB and more likely the result of the lenses focusing different frequencies into different depths on the waveguide face.
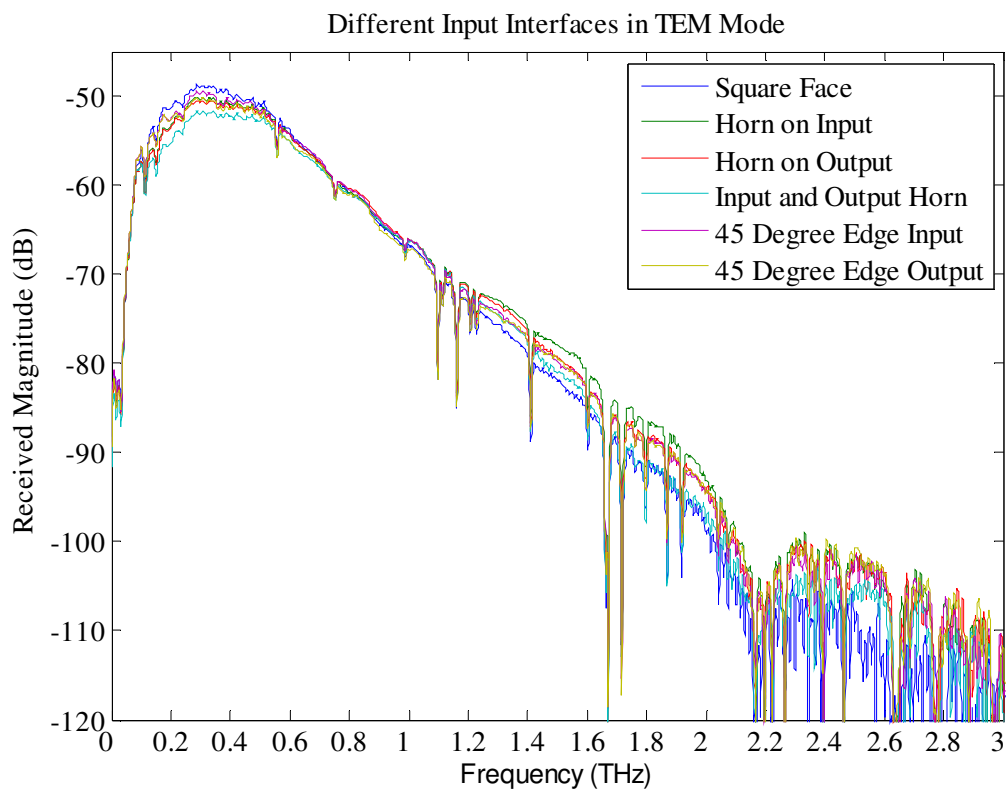
Figure IV.8: Comparison plot of different opening shapes, TEM mode

For the TE_1 mode plot of figure IV.9, one can notice that some of the horns seem to have a negative effect on the low-frequency cutoff. The most stable result appears to be the normal PPW flanged shape.

Different Input Interfaces in TE Mode
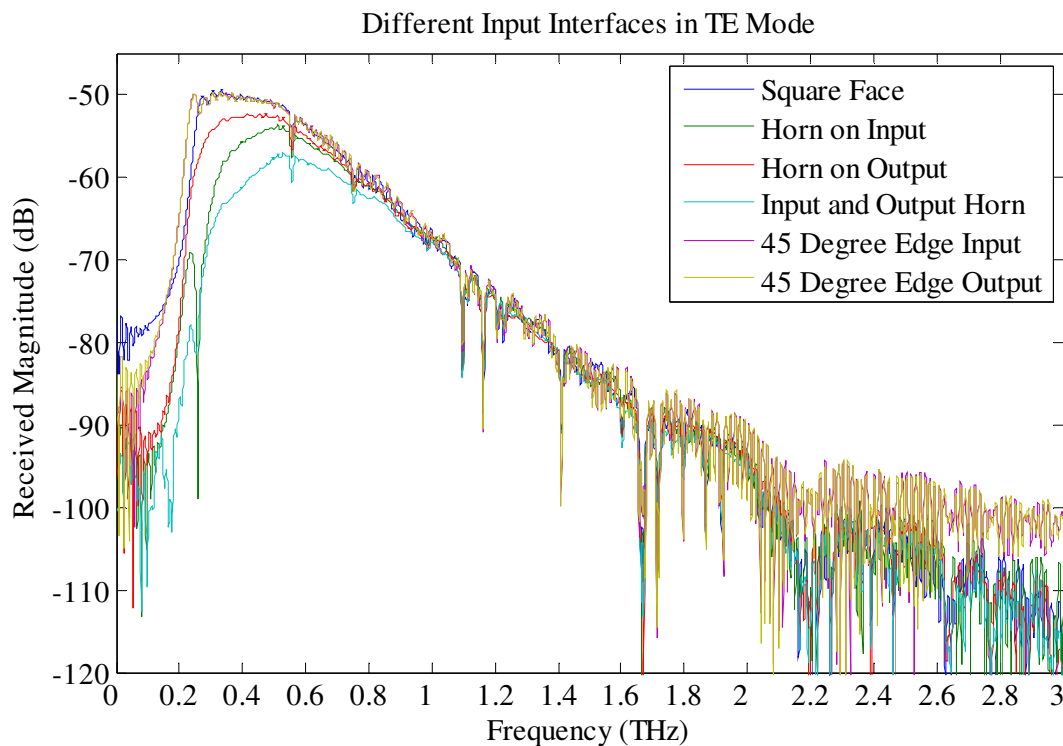
Figure IV.9: Comparison plot of different opening shapes, TE mode

The next set of experiments were on the horn plates that attached to the front of the

waveguide. The plates were aligned so that that small 1mm diameter hole on the output

was aligned perfectly with the input of the waveguide. As can be observed in the TEM

data of figure IV.10, there was about a 15dB loss in power over all frequency ranges,

along with a low frequency cutoff. This low frequency cutoff seems to point to another

propagation mode taking over once the THz radiation enters the horn. This in effect

filters the signal before it gets into the waveguide, and again on the way out. From this

TEM data, there is no advantage to using any kind of conical horns on input and/or

output, and the simple flanged input and output are the simplest and best in terms of

overall transmission coefficient.
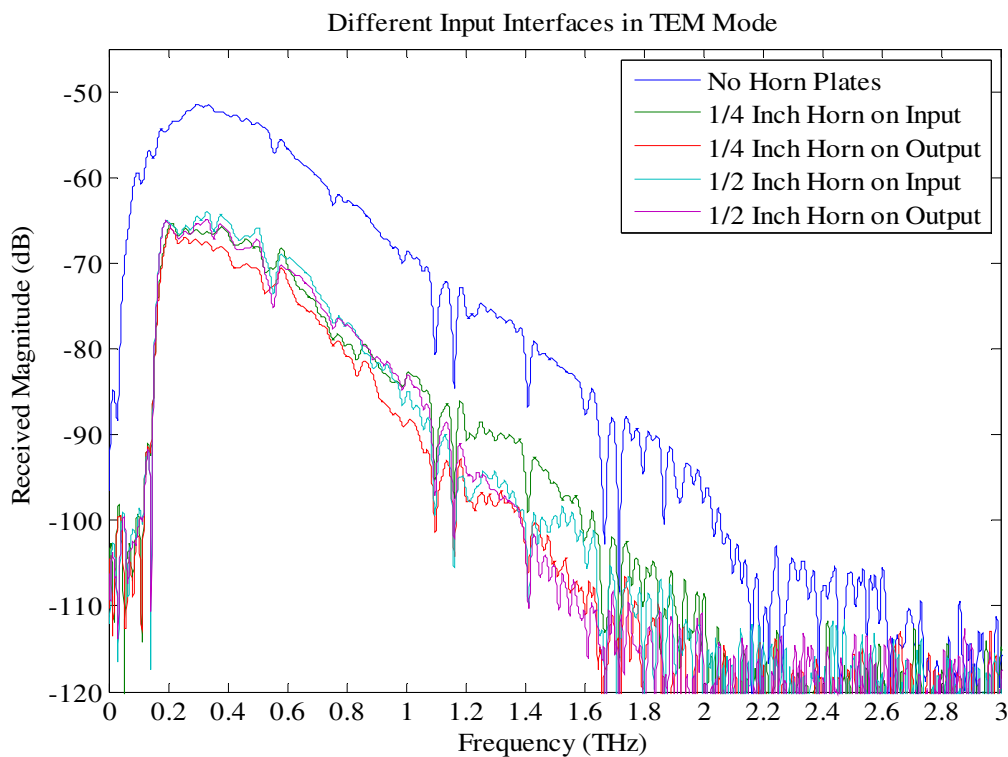
Figure IV.10: Comparison plot of conical shapes, TEM mode

In the TE data of figure IV.11, the results are better, with slightly less attenuation present, and no additional low-frequency cutoff. An explanation for this comes when the conical structure is approximated as a circular waveguide, which does not support TEM mode, but does support TE modes [3]. However, the same conclusion drawn from the TEM mode data still applies here, that there is no benefit to using conical structures on the input and/or output. All plots in figure IV.11 suffer from oscillations in the frequency domain for higher frequencies due to the lenses being too far apart (without the waveguide between them) and out of their optimal focal point ranges.

Different Input Interfaces in TE Mode
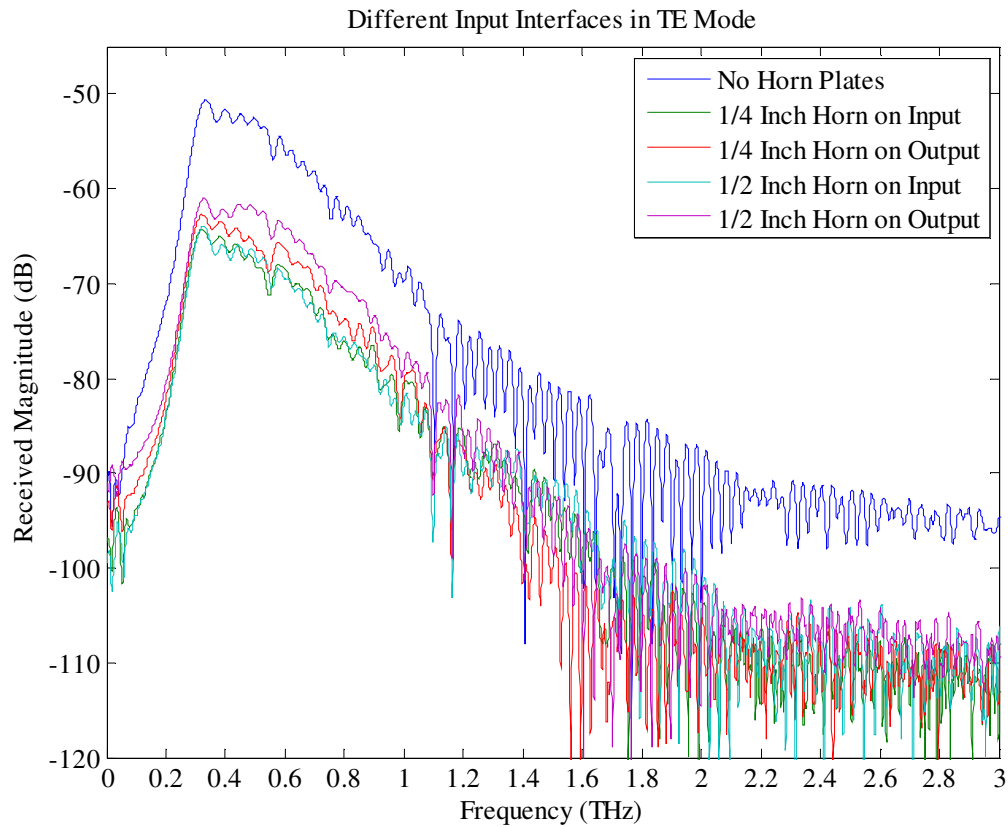
Figure IV.11: Comparison plot of conical shapes, TE mode

Because aligning the output hole on the input cone to the input hole on the output cone was such an issue, no data was taken with both a horn on the input and output. However, data with just the horns was taken and is shown in figure IV.12. As surmised above, the attenuation and low frequency cutoff is all caused by the horns, because the cutoffs remain without the waveguide in place.
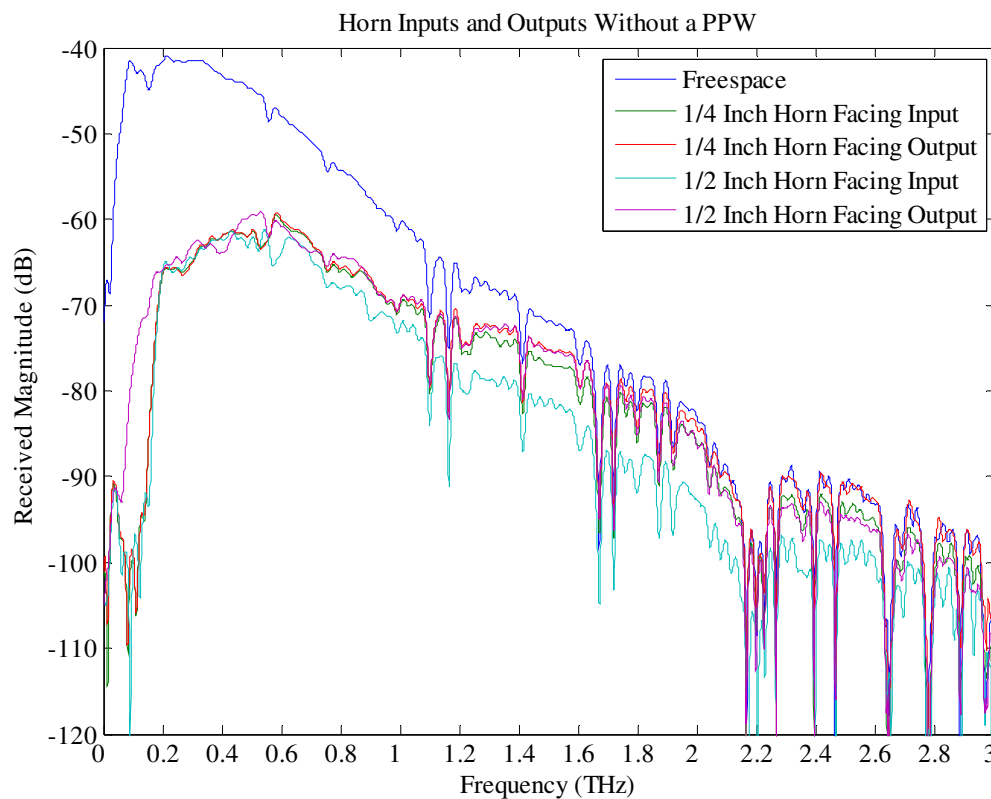
Figure IV.12: Measurement of the horn plates without the PPW

The conclusions taken from these measurements are that the easiest and simplest method

for measuring data with a waveguide is to use a simple square-faced waveguide.

However, more research may need to be done on having a very slightly angled input

spanning multiple wavelengths.

F.   Flexible Fixture

Data taken on the flexible waveguide was already shown above on the waveguide

spacing plots in figures IV.2 and IV.3.

G.   Resonator Waveguide

From the perspective of future uses of this work, design and understanding of the

operation of resonator waveguides is very important. For this thesis, only the basic

structure of a single groove was studied, with more complex structures planned for the

future.   It is necessary to use simulators in order to improve the understanding of the

resonator (the analytical expressions for such structures are complex), along with giving

the ability to design a resonator to fit the desired requirements, such as for a specific

resonant frequency. Therefore, establishing the credibility of the simulations by

comparing them to measured data is important in order to aide in the performance of

future designs.

The only data taken for the single-groove resonator waveguide was for TE_1 mode. This

is because groove is oriented parallel to the width of the waveguide, and interacts better

with the field of the TE_1 mode[4]. The data taken in the plots below yielded an

unexpected outcome. The notch (or resonant) frequency is not only a function of the

width of the channel cut into the waveguide, but also of the spacing between the

waveguide plates. It was additionally determined later by simulation that the notch frequency is also a function of the groove depth. The simulation low-frequency cutoff is much more severe than what is measured, so a calculated difference of a simulated reference waveguide minus a simulated grooved waveguide was used for the simulated data. This makes the simulated data appear to have no low-frequency cutoff, as evidenced in figure IV.15. This is not a cause for concern because the reason for these simulations was to determine the notch frequency. Figure IV.13 is for a waveguide spacing of 0.5mm, and it shows a good agreement between measured and simulated results. There is a small difference of 24GHz (or about 5%), which could be caused by several different factors, such as irregularities in the planarity of the waveguide, imperfect waveguide spacing, or the fact that the groove is not perfectly square (the bit used to machine it was slightly rounded). Initially, the major contributor to the error was thought to be caused by an error in the thickness of the bit (which affects groove width), but changing the groove width in the simulation by 5% only yielded a 1.5% change in notch frequency. Additionally, from table IV.6, one can see that a 20% increase in waveguide spacing from 0.5mm to 0.6mm yields a 10% decrease in notch frequency. Another parameter adjusted in simulation was the groove depth, and a 10% increase of the depth yielded a 1.7% decrease in notch frequency From this, one can surmise that a small error in the waveguide spacing or notch width should not have a large affect on the notch frequency. Because of these three observations, and the fact that simulation matches measurement much better for smaller spacings, it is believed that the source of error is caused by MEEP, and not an error in the measurement fixture.

69

If one compares figures IV.13, IV.14, and IV.15 together, there are also other notches at

0.557 and 0.752THz which do not appear in the simulated data. These frequencies are

due to water vapor, and are also given in table I.1
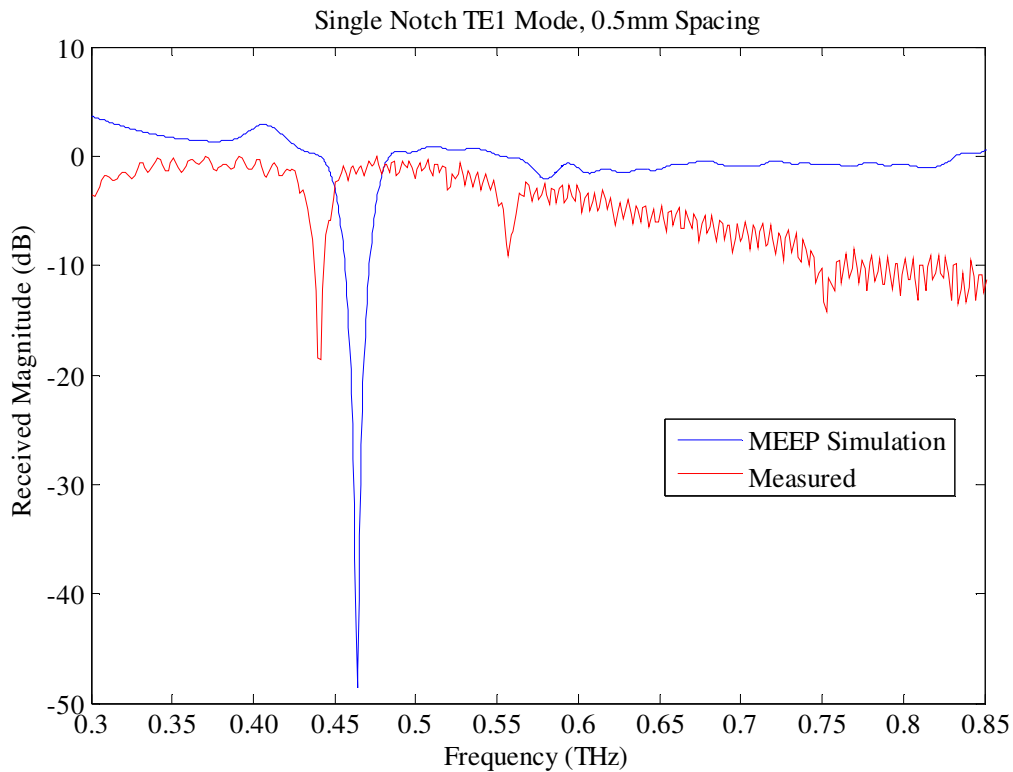
Figure IV.13: Simulation vs. Measured For PPW with Groove and 0.5mm Spacing

Figure IV.14 is for a spacing of 0.6mm. Once again, the measured notch frequency is

slightly less than simulated.
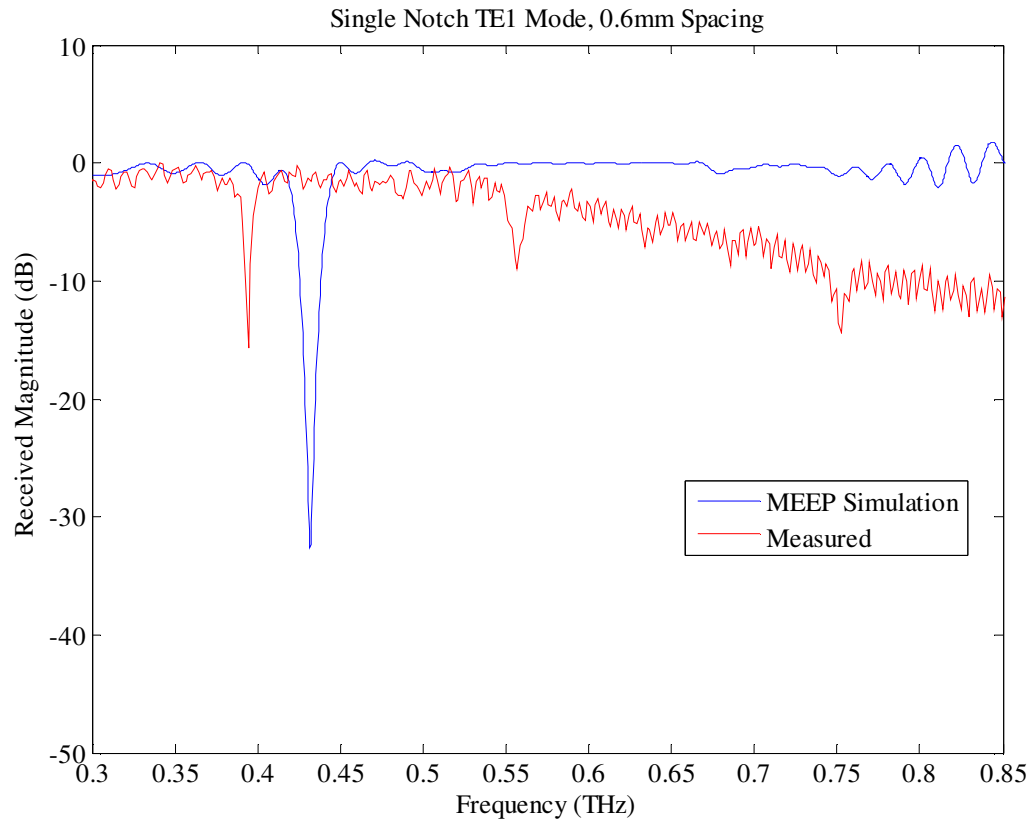
Figure IV.14: Simulation vs. Measured For PPW With Groove and 0.6mm Spacing

The final plot for a waveguide spacing of 0.38mm is shown in figure IV.15. As mentioned previously, the low-frequency cutoff does not appear on the simulated data, as evidenced in this figure. The main notch increases in frequency as would be expected from the previous data of the 0.5mm and 0.6mm spacings, but two other notches appear in the simulation. The first notch appears in the measured data, but there is no third notch. The measured notch that is close to the third simulated notch is the same one that appeared in figures IV.13 and IV.14, and is not caused by the machined groove. It is not known with certainty why this third notch did not appear in the measured data, but with a

spacing of 0.38mm, the measurements are taking place with a received power close to the noise floor (as evidenced by the SNR comparisons for 0.3 to 0.5mm spacing in figure IV.3). The notch may simply be too "shallow" to be observed and it may also be too close to a known vapor absorption line to be detectable.

Single Notch TE1 Mode, 0.38mm Spacing
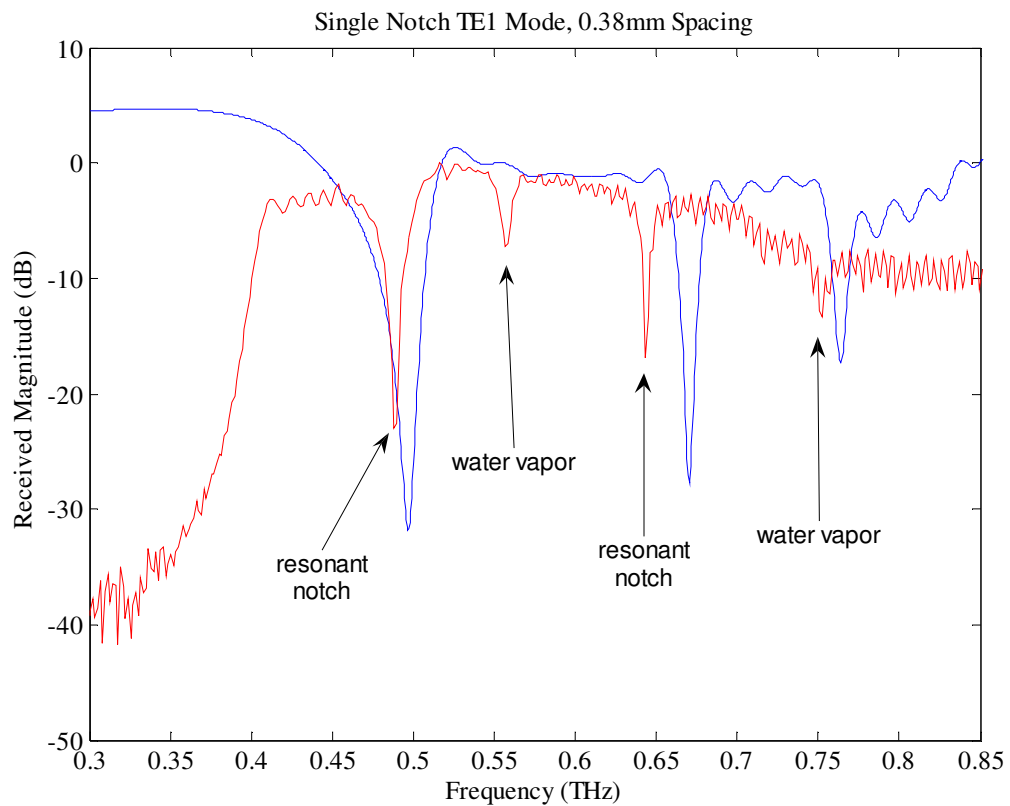
Figure IV.15: Simulation vs. Measured For PPW With Groove and 0.38mm Spacing

Table IV.6 gives the simulated versus measured notch frequencies for all three simulations.

Table IV.6: Simulated vs. Measured Notch Values

Spacing (mm)	Simulated (GHz)	Measured (GHz)	Difference (GHz)
0.38	495.7	489.8	5.9
0.5	463.7	439.7	24
0.6	432.2	394.3	37.9

From the above data, it appears as though the MEEP simulations do not provide enough

accuracy to be used to predict fine features of the measured resonator and of future

similar designs. This is critical because manufacturing of the resonators is currently slow

and relatively expensive process. More exploration of the simulation approximations will

be necessary before MEEP can be reliably used for designing resonators. This simulation

approach should also be compared with other simulation programs since there is some

variability among them as well. However, it has been established that experimentally

observed resonances can be accurately and reliably measured but interpretation and

analysis of the results need further work.

V.   Conclusions

The field of THz study continues to grow, and the steps taken in this thesis will help the further continuation of research at the NEAR lab. In this paper, many different configurations have been characterized, and a flexible fixture was also developed for future work in the THz field. Different openings and exits to the waveguide were tested out, with the results pointing to a normal flanged input/output being the most useful configuration. Both the TEM/TM$_0$ and lowest order TE$_1$ propagation modes were used to characterize these devices, and the advantages and disadvantages of each mode were discussed. Both of these modes were tested out with different opening heights, and it was found that an ideal opening for both transmission modes was around 0.8mm. Waveguides of different polishes were tested along with gold coating, and it was found that having a highly polished surface does slightly aid in PPW transmission, while the results of gold plating were inconclusive due to the gold layer being too thin. Additionally, a basic resonator structure was built and compared to simulations, showing that it is possible to get areas of resonance in a waveguide similar to simulations. Based on the work described in this thesis, the next steps in THz measurement at Portland State University will be achievable.

A.   Final Waveguide Design

The final waveguide designed and used for measuring transmitted power vs. opening height met the design requirements of being low-cost, accurate, able to make repeatable measurements, and be easy to use. This design, or variations of it, is already being used in further research by other students at Portland State University. It has been demonstrated that the waveguide can handle measurements in both TEM and TE_1 propagation modes, as well as be used in conjunction with lenses. The waveguide setup has also been used with success in the Virgina Diodes continuous wave system. Thus, the waveguide design should prove useful for a variety of planned projects in the THz lab.

B.   Applications of Current Work

As more complicated measurements are performed in the NEAR lab, it is extremely important to have familiarity with the fundamentals of the equipment, the setup, and measurement methods. This is why the exploratory work done was an important step to take. The work done also verifies a lot of papers written by other THz researchers, which is important as it lends credibility to the research. It was also interesting to note that the signal-to-noise ratio of the measurements taken at Portland State University were superior to that of many other papers[4][9][10].

C.   Important Lessons Learned

The most important things learned are the guidelines for fabricating future fixtures, knowing what does and does not work with the shape of the fixture, and how to properly take useful data with the best possible signal to noise ratio. Another important thing learned was the ability to identify which propagation mode was dominating in the waveguide by looking at the time domain or frequency domain data.

VI.   Future Work

This chapter details a few of the potential future areas of research using the information

learned in this thesis. The flexible fixture, or some variation of it, developed during the

course of this thesis should be usable for most of the future work listed below.

A.   Expanded Use of Resonators

Resonators present a very promising use for waveguides, because they have the ability to

filter out certain frequencies, as well as concentrate the power of certain frequencies at a

specific place in the waveguide. This concept was demonstrated in [9]. In this paper,

metalized silicon with periodic groove structures were used instead of a normal

waveguide. A side view of the setup is shown in the figure VI.1.
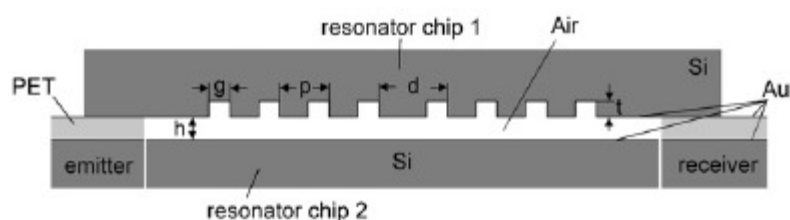
Figure VI.1: Side view of resonator structure [9]

This allowed a much higher sensitivity to the biological molecules being characterized,

due to the larger concentration of energy in the waveguide, as shown in the figure VI.2.
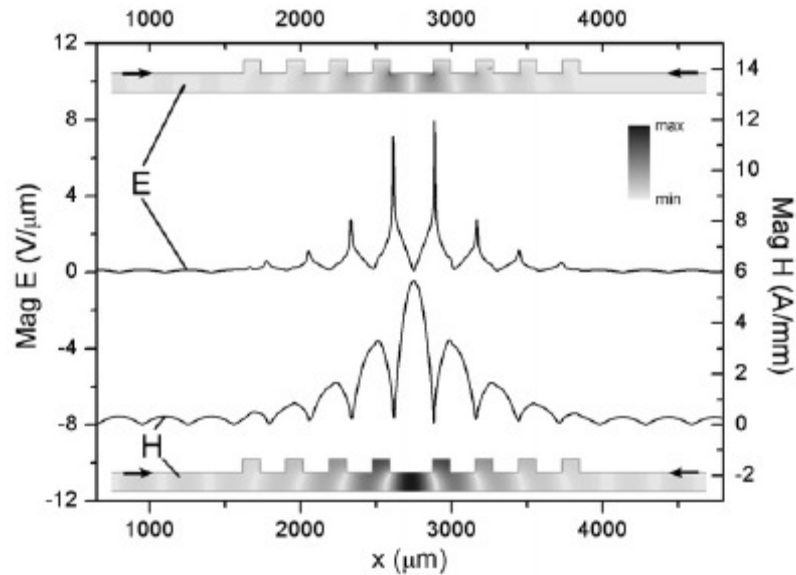
Figure VI.2: Power vs. location on resonator [9]

Values used for the width of the notches were 112μm, and they were 93 μm deep.

Although this was used for biological samples, a similar setup could potentially be used

to characterize other materials. Before resonators of the type described can be machined

however, better simulation methods need to be explored. It can be very expensive and

time consuming to create such resonators unless one knows exactly how they will

function. This will be the next step after the initial data taken on the single notch detailed

in chapter IV.

B.   Materials Sensing in a Waveguide

One area not explored too much in this thesis was to put different materials in the

waveguide and see what effect they have on the output spectrum. A number of

interesting experiments could be performed on finding the amount of a material necessary to accurately detect it in a waveguide versus in free space. These experiments could also be combined with the information learned about the resonator structure mentioned above.

C.   Different Waveguide Materials

Taking data with a waveguide with a thicker coating of gold on it would be a worthwhile exercise. The thickness of the gold coating should at least be several skin depths, or around 250nm, to take an effective measurement. Another useful material to build a PPW out of could be copper, which has a high conductivity and higher melting point than aluminum.

D.   Nano-Materials in a Waveguide

Nano-materials have many future uses, such as nano-wire gate transistors, ultraviolet LEDs, and lasers. One problem is that it is very hard to characterize them. Fortunately, THz radiation can be used to do this. Nano materials such as zinc oxide and titanium oxide can be grown on a plate and exposed to radiation to determine such parameters as index of refraction, absorption, and conductivity. The waveguide designed in this thesis is well suited to this task due to the modularity of its design. Nano-wires can be grown on an aluminum block with the holes already machined into it, and used in the setup.
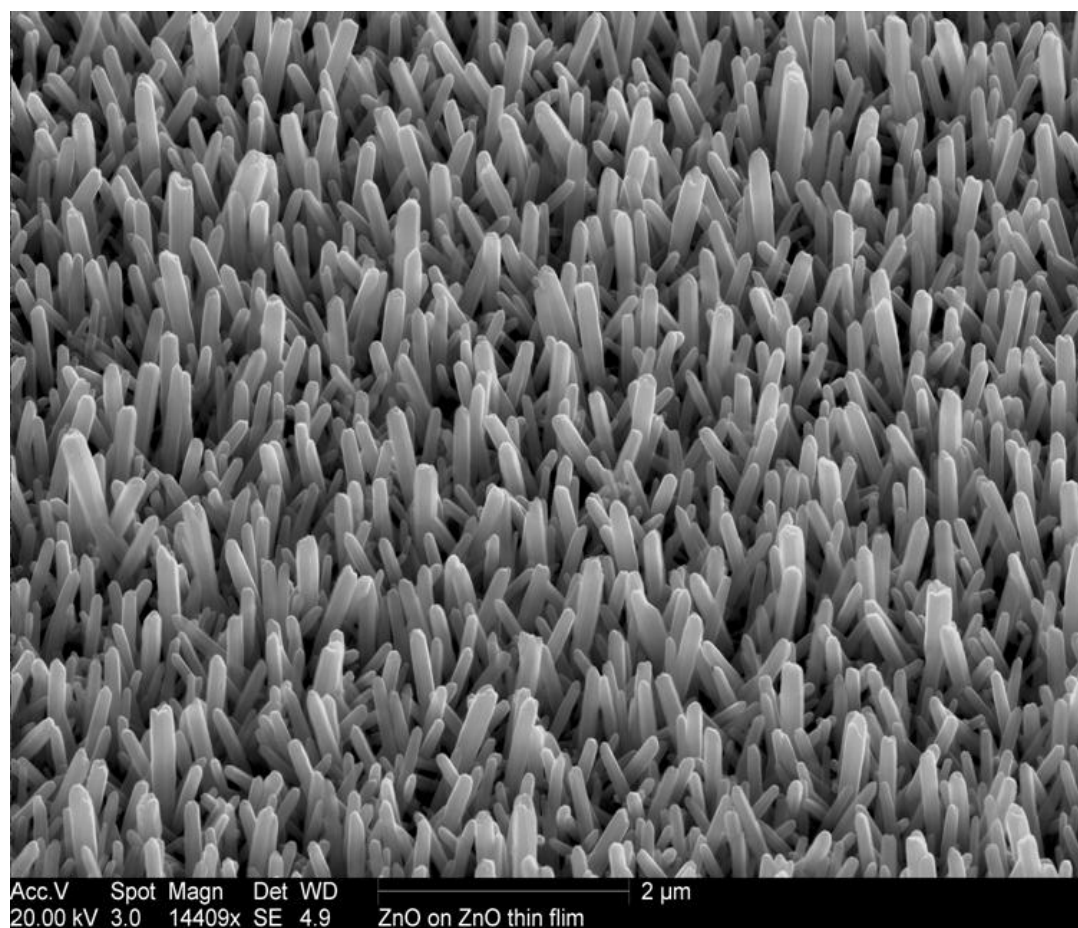
Figure VI.3: SEM image of ZnO nano-wires

References

[1]   R. Mendis, "Nature of subpicosecond terahertz pulse propagation in practical dielectric-filled parallel-plate waveguides", Optics Letters, vol. 31, no. 17, pp. 2643-2645, 2006.

[2]   R. Mendis and D. Grischkowsky, "Undistorted guided-wave propagation of subpicosecond terahertz pulses," Optics Letters, vol. 26, no. 11, pp. 846-848 (2001).

[3]   D. M. Pozar, *Microwave Engineering,* (Wiley, 2005).

[4]   R. Mendis and D. M. Mittleman, "Comparison of the lowest-order transverse-electric (TE$_1$) and transverse-magnetic (TEM) modes of the parallel-plate waveguide for terahertz pulse applications", Optics Express, vol. 17, no. 17, pp. 14839-14850, 2009.

[5]   R. Mendis and D. M. Mittleman, "An investigation of the lowest-order transverse-electric (TE$_1$) mode of the parallel-plate waveguide for THz pulse propagation", Journal of the Optical Society of America, vol. 26, no. 9, pp. A6-A13, 2009.

[6]   E. S. Lee, J. S. Jang, S. H. Kim, Y. B. Ji, and T. Jeon, "Propagation of Single-Mode and Multi-Mode Terahertz Radiation Through a Parallel-Plate Waveguide", Journal of the Korean Physical Society, vol. 53, no. 4, pp. 1891-1896, 2008.

[7]   C. A. Balanis, *Antenna Theory,* (Wiley, 2005).

[8]   T. Jeon and D. Grischkowsky, "Characterization of optically dense, doped

semiconductors by reflection THz time domain spectroscopy", Applied Physics

Letters, vol. 72, no. 23, pp. 3032-3034, 1998.

[9]   M. Nagel, P. H. Bolivar, and H. Kurz, "Modular parallel-plate THz components

for cost-efficient biosensing systems", Semiconductor Science and Technology,

vol. 20, pp. S281-S285, 2005.

[10]   R. Mendis, V. Astley, J. Liu, and D. M. Mittleman, "Terahertz microfluidic

sensor based on parallel-plate waveguide resonant cavity", Applied Physics

Letters, vol. 95, no. 171113.

[11]   A. Bingham, Y. Zhao, and D. Grischkowsky, "THz parallel plate photonic

waveguides", Applied Physics Letters, vol. 87, no. 051101, 2005.

[12]   R. Menids and D. Grischkowsky, "THz Interconnect With Low-Loss and Low-

Group Velocity Distortion", IEEE Microwave and Wireless Components Letters,

vol. 11, no. 11, pp. 444-446, 2001.

[13]   E. S. Lee and T. Jeon, "THz Filter Using the Transverse-electric (TE$_1$) Mode of

the Parallel-plate Waveguide", Journal of the Optical Society of Korea, vol. 13,

no. 4, pp. 423-427, 2009.

[14]   G. Gallot, S. P. Jamison, R. W. McGowan, and D. Grischkowsky, "Terahertz waveguides", Journal of the Optical Society of America, vol. 17, no. 5, pp. 851-863, 2000.

[15]   J. S. Melinger, S. S. Harsha, N. Lamen, and D. Grischkowsky, "Guided-wave terahertz spectroscopy of molecular solids", Journal of the Optical Society of America, vol. 26, no. 9, pp. A79-A89, 2009.

[16]   Y. S. Lee, *Principles of Terahertz Science and Technology*, (Springer, 2009).

[17]   M. Exter, Ch. Fattinger, d. Grischkowsky, "Terahertz time-domain spectroscopy of water vapor", Optics Letters, vol. 14, no. 20, pp. 1128-1130, 1989.

VII.   Appendices

A.   MEEP Simulation Script

```
;Parallel-Plate Waveguide with .38mm square groove
;All units normalized to the .38mm notch size
;PPW length is 19mm --> 50 units
;PPW opening is 0.5mm ---> 1.3158 units  \
;Notch center is wwidth/2 + .5 ---> 1.1579 units
;sy must be greater than 2*(wwidth/2 + 1) ---> 3.3158 units

;Set center frequency at about 591GHz ---> ((meep_scale =
.38mm)*591GHz)/c ~= 1
;Span from 39GHz to 1.14THz ---> = c/((meep_scale = .38mm)*(1/(0.75 +/-
0.7)))

(define-param sx 62)
(define-param sy 5)
(set! geometry-lattice (make lattice (size sx sy no-size)))

(define-param wlength 50) ; length of waveguide
(define-param wwidth 1.3158) ; width of waveguide

(define-param fcen 0.75)
(define-param df 1.4)
(define-param nfreq 2000)
(define-param dpml 5)


(set! pml-layers (list (make pml (thickness dpml) (direction X))))
(set-param! resolution 60)

(set! geometry
      (list
       (make block
         (center 0 0)
         (size wlength infinity infinity)
         (material (make dielectric (epsilon -10e16))))
       (make block
         (center 0 0)
         (size infinity wwidth infinity)
         (material air))
       (make block
         (center 0 1.1579)
         (size 1 1 infinity)
         (material air))
      )
)


(begin
(set! sources (list
            (make source
```

```
              (src (make gaussian-src (frequency fcen) (fwidth df)))
              (component Ez)
              (center (+ dpml (* -0.5 sx)) 0)
              (size 0 5))))


(define trans ; transmitted flux
      (add-flux fcen df nfreq
       (make flux-region
         (center (- (* 0.5 sx) dpml 0.5) 0) (size 0 (* 2 wwidth)))))))

(use-output-directory)

(run-until 100
           (at-beginning output-epsilon)
           (at-end output-hfield-y)
         (at-every 1 (output-png Ez "-Zc dkbluered"))
          ;(to-appended "hy" (at-every 0.1 (in-volume (volume (center
9 0)) output-hfield-y))))
)

(display-fluxes trans)
)
```